Mon. Not. R. Astron. Soc. **315**, 184–208 (2000)

The stellar populations of early-type galaxies in the Fornax cluster

Harald Kuntschner★
University of Durham, Department of Physics, South Road, Durham DH1 3LE

Accepted 2000 January 17. Received 2000 January 17; in original form 1999 August 4

ABSTRACT

We have measured central line strengths for a magnitude-limited sample of early-type galaxies in the Fornax cluster, comprising 11 elliptical (E) and 11 lenticular (S0) galaxies, more luminous than $M_B = -17$. When compared with single-burst stellar population models we find that the centres of Fornax ellipticals follow a locus of fixed age and have metallicities varying roughly from half solar to twice solar. The centres of (lower luminosity) lenticular galaxies, however, exhibit a substantial spread to younger luminosity-weighted ages, indicating a more extended star formation history.

Galaxies with old stellar populations show tight scaling relations between metal-line indices and the central velocity dispersion. Remarkably also, the Fe lines are well correlated with σ_0. Our detailed analysis of the stellar populations suggests that these scaling relations are driven mostly by metallicity. Galaxies with a young stellar component do generally deviate from the main relation. In particular, the lower luminosity S0s show a large spread.

Our conclusions are based on several age/metallicity diagnostic diagrams in the Lick/IDS system comprising established indices such as Mg_2 and $H\beta$ as well as new and more sensitive indices such as $H\gamma_A$ and Fe3, a combination of three prominent Fe lines. The inferred difference in the age distribution between lenticular and elliptical galaxies is a robust conclusion, as the models generate consistent relative ages using different age and metallicity indicators, even though the absolute ages remain uncertain. The absolute age uncertainty is mainly caused by the effects of non-solar abundance ratios which are not yet accounted for by the stellar population models. Furthermore, we find that elliptical galaxies and the bulge of one bright S0 are overabundant in magnesium, where the most luminous galaxies show the strongest overabundances. The stellar populations of young and faint S0s are consistent with solar abundance ratios or a weak Mg underabundance. Two of the faintest lenticular galaxies in our sample have blue continua and extremely strong Balmer-line absorption, suggesting star formation <2 Gyr ago.

Key words: galaxies: abundances – galaxies: clusters: individual: Fornax – galaxies: elliptical and lenticular, cD – galaxies: formation – galaxies: kinematics and dynamics.

1 INTRODUCTION

Great efforts have been made in the last few years to develop evolutionary stellar population synthesis models (Bruzual & Charlot 1993; Worthey 1994, hereafter W94; Weiss, Peletier & Matteucci 1995; Vazdekis et al. 1996, hereafter V96; Kodama & Arimoto 1997) in order to analyse the integrated light of galaxies and derive estimates of their mean ages and metal abundances. One of the main obstacles in the interpretation has been the age/metallicity degeneracy in old stellar populations. As pointed out by W94 the integrated spectral energy distribution (SED) of an old (>2 Gyr) stellar population looks almost identical when the age is doubled and total metallicity reduced by a factor of 3 at the same time. Therefore two galaxies with almost identical broad-band colours can have significantly different ages and metallicities. In the optical wavelength range, only a few narrow-band absorption-line-strength indices and the 4000-Å break (see also Gorgas et al. 1999) have so far been identified which can break this degeneracy.

One of the most successful and widely used methods for measuring the strength of age/metallicity discriminating absorption features is the Lick/IDS system (Burstein et al. 1984; Worthey et al. 1994; Trager et al. 1998), which has been used by many authors (Davies, Sadler & Peletier 1993; González 1993; Fisher, Franx & Illingworth 1995, 1996; Ziegler & Bender 1997; Longhetti et al. 1998; Mehlert 1998; Jørgensen 1999). In contrast with high-resolution-index systems (Rose 1994; Jones & Worthey 1995), which promise a better separation of age and metallicity, the Lick/IDS system allows the investigation of dynamically hot

★ E-mail: harald.kuntschner@durham.ac.uk

galaxies that have intrinsically broad absorption lines. By plotting an age-sensitive index and a metallicity-sensitive index against each other, one can (partially) break the age/metallicity degeneracy and estimate, with the help of model predictions, the luminosity-weighted age and metallicity of an integrated stellar population (see Fig. 4). Most recently, Jørgensen (1999) used this methodology to investigate the stellar populations of a large sample of early-type galaxies in the Coma cluster. She concluded that there are real variations in both the ages and the abundances, while an anticorrelation between the mean ages and the mean abundances makes it possible to maintain a low scatter in scaling relations such as Mg–σ_0. Colless et al. (1999) present similar conclusions from the analysis of a combination of the Mg–σ_0 relation and the Fundamental Plane in a large sample of cluster early-type galaxies.

The spread in the ages for early-type galaxies and the anti-correlation of age and metallicity found by the previous authors supports the hierarchical picture for the construction of galaxies in which galaxies form via several mergers involving star formation (Baugh, Cole & Frenk 1996; Kauffmann 1996). However, the results are inconsistent with the conventional view that all luminous elliptical galaxies are old and coeval. In the conventional picture the global spectrophotometric relations observed for ellipticals, for example the colour–magnitude relation (Visvanathan & Sandage 1977; Bower, Lucey & Ellis 1992; Terlevich 1998), are explained by the steady increase in the abundance of heavy elements with increasing galaxy mass. This increase arises naturally in galactic wind models such as that of Arimoto & Yoshii (1987) and Kodama & Arimoto (1997).

Although with line-strength indices we can (partially) break the age/metallicity degeneracy, this is by no means the last obstacle to overcome on our way to fully understand the stellar populations of early-type galaxies and the cause of scaling ralations. Since the late 1970s, evidence has been accumulating that abundance ratios in galaxies are often non-solar. In particular, the magnesium-to-iron ratio seems to be larger in luminous early-type galaxies when compared to solar-neighbourhood stars (O'Connell 1976; Peletier 1989; Worthey, Faber & González 1992; Davies et al. 1993; Henry & Worthey 1999; Jørgensen 1999). However, with only a very few exceptions (e.g., Weiss et al. 1995), non-solar abundance ratios have not yet been incorporated in the model predictions. Among other issues this seems to be the most important single problem which prevents us from deriving accurate *absolute* age and metallicity estimates from integrated-light spectroscopy (Worthey 1998). Nevertheless, with the current models and high S/N data we are able to study relative trends in ages and abundances, as well as start to investigate the effects of non-solar abundance ratios for individual elements (Worthey 1998; Peletier 2000).

In this paper, high S/N nuclear spectra of a complete sample of early-type galaxies in the Fornax cluster brighter than $M_B = -17$ are analysed in the Lick/IDS system. The early results of this study have already been presented in a letter to this journal (Kuntschner & Davies 1998). This paper is organized as follows. Section 2 describes the sample selection and basic data reduction. The calibration of the line-strength indices to the Lick/IDS system is presented in Section 3 and Appendix B. Section 4 presents a consistency test for the model predictions and our measured line-strength indices. In Section 5 several index combinations are compared to model predictions. In particular, the effects of non-solar abundance ratios, composite stellar populations and age/metallicity estimates of the integrated light are discussed. In Section 6 observed index–σ_0 relations are presented. Relations between derived parameters such as age, metallicity and [Mg/Fe] with the central velocity dispersion are investigated in Section 7. We then discuss the implications of our results in Section 8, and present our conclusions in Section 9. The fully corrected Lick/IDS indices of our sample are tabulated in Appendix B.

Table 1. The instrumental set-up.

Telescope	AAT (3.9 m)
Dates	6–8 December 1996
Instrument	RGO spectrograph
Spectral range	4243–5828 Å
Grating	600 V
Dispersion	1.55 Å pixel^{-1}
Resolution (FWHM)	~4.1 Å
Spatial Scale	0.77 arcsec pixel^{-1}
Slit Width	2.3 arcsec
Detector	Tek1k #2 (24 μm^2 pixels)
Gain	1.36 e$^-$ ADU^{-1}
Read-out noise	3.6 e$^-$ rms
Seeing	~1″

2 THE OBSERVATIONS AND DATA REDUCTION

2.1 The sample

Our sample of 22 early-type galaxies has been selected from the catalogue of Fornax galaxies (Ferguson 1989, hereafter F89), in order to obtain a complete sample down to $B_T = 14.2$ or $M_B = -17$.[1] We have adopted the morphological classifications given by F89, and checked them with images we obtained on the Siding Spring 40-inch telescope. From these we noted a central dust lane in ESO 359-G02 and a central disc in ESO 358-G59, which led us to classify them as lenticular galaxies. NGC 1428 was not observed because of a bright star close to its centre. We also added the elliptical galaxy IC 2006 to our sample, as it was not classified by F89. The bona fide elliptical NGC 3379 was observed as a calibration galaxy. The observations were carried out with the AAT (3.9 m) on the nights of 1996 December 6–8 using the RGO spectrograph. The characteristics of the detector and the instrument set-up are given in Table 1.

Typically, exposure times were between 300 and 1800 s per galaxy (see Table 2 for a detailed listing). For most of the observations the slit was centred on the nucleus at PA = 90°. The seeing was generally better than 1 arcsec. Additionally, we observed 15 different standard stars (mainly K-giants) during twilight to act as templates for velocity dispersion measurements, as well as to calibrate our line-strength indices to the Lick/IDS system (Worthey et al. 1994). The spectrophotometric standard stars GD 108 and L745-46A were observed to enable us to correct the continuum shape of our spectra. Table 3 lists all observed standard stars with their spectral types (obtained from SIMBAD, operated by CDS, Strasbourg) and also comments on their use as Lick/IDS standard, velocity standard or spectrophotometric standard.

2.2 Basic data reduction

Most of the basic data reduction steps have been performed with packages under IRAF. For each night individually the science

[1] Adopting a distance modulus of $m - M = 31.2$, based on *I*-band surface brightness fluctuations (Tonry et al. 1997).

Table 2. Log of observations: galaxies.

Galaxy	Type	B_T [mag]	Exp. time [s]	PA [°]
NGC 1316	S0 pec	9.4	300	90
NGC 1336	E4	13.1	1200	90
NGC 1339	E4	12.5	600	90
NGC 1351	E5	12.5	900	90
NGC 1373	E3	14.1	1200	90
NGC 1374	E0	12.0	900	90
NGC 1375	S0	13.2	900	90
NGC 1379	E0	11.8	600	90
			600	90
NGC 1380	S0	10.9	300	90
NGC 1380A	S0	13.3	900	90
NGC 1381	S0	12.4	480	90
			900	140
			900	50
NGC 1381[a]	S0		1800	50
NGC 1399	E0, cD	10.6	300	90
			600	181
NGC 1404	E2	11.0	300	90
			300	90
NGC 1419	E0	13.5	1200	90
NGC 1427	E4	11.8	600	90
			1800	79
			1800	169
IC 1963	S0	12.9	600	90
IC 2006	E	12.2	600	90
ESO 359-G02	S0	14.2	1200	90
ESO 358-G06	S0	13.9	1800	90
ESO 358-G25	S0 pec	13.8	1200	90
ESO 358-G50	S0	13.9	1200	90
ESO 358-G59	S0	14.0	1200	90
NGC 3379[b]	E1	10.2	300	90

Notes – [a] offset from nucleus; [b] calibration galaxy, non-Fornax member.

Table 3. Log of observations: stars.

Name	Type	comment
HD 004656	K4IIIb	Lick/IDS std
HD 037160	K0IIIb	Lick/IDS std
HD 040657	K1.5III	velocity std
HD 047205	K1III	Lick/IDS std
HD 050778	K4III	Lick/IDS std
HD 054810	K0III	Lick/IDS std
HD 058972	K3III	Lick/IDS std
HD 061935	G9III	Lick/IDS std
HD 066141	K2III	Lick/IDS std
HD 071597	K2III	velocity std
HD 083618	K2.5III	Lick/IDS std
HD 088284	K0III	Lick/IDS std
HD 095272	K1III	Lick/IDS std
HD 219449	K0III	Lick/IDS std
HD 221148	K3III variable	Lick/IDS std
L745-46A	DF	spec. std (Oke 1974)
GD 108	sd:B	spec. std (Oke 1990)

frames were overscan-corrected and a bias frame was subtracted. A few bad columns were removed by linear interpolation. From several domeflats and skyflats a final flat-field accounting for the pixel-to-pixel variations and vignetting was constructed and applied to the frames. Cosmic rays were removed using the `cleanest` task in the `REDUCEME` package (Cardiel et al. 1998). This task automatically detects and removes cosmic rays via a sophisticated deviation algorithm, while at the same time one can interactively inspect potential cosmic rays in sensitive areas such as close to the galaxy centre. The wavelength solution was determined from Th-Ar-lamp spectra which were taken before and after most of the science observations. The rms residual in the wavelength fit was typically 0.1–0.2 Å. Finally, the sky was subtracted.

The central spectrum for each galaxy was extracted by fitting a low-order polynomial to the position of the centre along the wavelength direction, re-sampling the data in the spatial direction, and finally co-adding the spectra within a 5-pixel aperture yielding an effective aperture of $2.3 \times 3.85\,\mathrm{arcsec}^2$. Multiple exposures of the same galaxy were combined. The resulting S/N in the spectra ranges from $\sim$30 [Å^{-1}] for the faintest galaxies to more than 100 [Å^{-1}] for the brightest ones (measured in a $\sim$100-Å-wide region just bluewards of the Mg b feature). For stars we used the `IRAF` task `apall` to extract 1D spectra. All galaxy and stellar spectra were logarithmically rebinned to a common wavelength range and increment. Finally, the continuum shape of our spectra was corrected to a relative flux scale with the help of the spectrophotometric standard stars.

2.3 Kinematics

In order to correct the line-strength indices for velocity dispersion broadening and to construct index–σ_0 relations, we need to measure the central velocity dispersion for each galaxy. Estimates were derived with the Fourier correlation quotient (FCQ, version 8) method (Bender 1990; Bender, Saglia & Gerhard 1994). For the FCQ analysis the spectra were rebinned to twice the original spectral sampling, and a wavelength range of 4876 to 5653 Å was extracted. Note that the Hβ feature is excluded from the wavelength range, as it proved to be a source of severe template mismatch for galaxies with strong Balmer absorption. As we consider only central spectra in this paper, we fit a pure Gaussian profile to the broadening function, neglecting higher order terms. To check the reliability of the FCQ analysis, we used eight different G- and K-giant template stars. For galaxies with a central velocity dispersion of $\sigma_0 \geq 70\,\mathrm{km\,s^{-1}}$, all eight template stars give very similar results, and an average value was adopted. The rms scatter between different template stars is 0.007 in log units for galaxies with $\sigma_0 \geq 100\,\mathrm{km\,s^{-1}}$. For galaxies with $70 \leq \sigma_0 < 100\,\mathrm{km\,s^{-1}}$ the rms scatter increases to 0.024, and for galaxies with $\sigma_0 < 70\,\mathrm{km\,s^{-1}}$ we find an rms scatter of 0.074. The uncertainty introduced by different template stars was comparable to or larger than the internal error estimates of the FCQ program. Note that for galaxies with $\sigma_0 < 70\,\mathrm{km\,s^{-1}}$ some template stars gave a poor fit to the broadening function and were excluded from the template sample. Only remaining measurements were averaged.

Using this procedure, velocity dispersions as low as $\sim$50 km s^{-1} could be recovered, although systematic errors will start to dominate for $\sigma_0 < 90\,\mathrm{km\,s^{-1}}$. As our spectral resolution is rather low compared to velocity dispersions of $\sim$50–60 km s^{-1}, we emphasize that for these faint galaxies our velocity dispersions are only rough estimates. The final velocity dispersion errors for galaxies with $\sigma \geq 70\,\mathrm{km\,s^{-1}}$ ($\Delta \log \sigma_0 = 0.022$) were derived by a literature comparison (see Appendix A, Fig. A1). For galaxies with $\sigma_0 < 70\,\mathrm{km\,s^{-1}}$ we adopt the mean rms scatter of the template stars ($\Delta \log \sigma_0 = 0.074$).

3 LICK/IDS CALIBRATION

The wavelength range of our spectra covers 16 different line-strength indices, such as Mg_2, Hβ and Hγ_A, in the Lick/IDS

system which is described in detail in W94, Worthey & Ottaviani (1997, hereafter WO97) and Trager et al. (1998). In the following analysis we use an updated version of the W94 models which is available from Dr. G. Worthey's home page. The updates affect only models where [Fe/H] ≤ -1.0. and are most noticable for the Hβ index. For a recent study of the behaviour of the Balmer indices at low metallicities see Poggianti & Barbaro (1997) and Maraston, Greggio & Thomas (2000). Before one can compare the measured indices with model predictions by, e.g., W94 and V96, the measurements have to be carefully calibrated to the Lick/IDS system. Generally there are three effects to account for: (a) the difference in the spectral resolution between the Lick/IDS system and our set-up, (b) the internal velocity broadening of the observed galaxies, and (c) small systematic offsets caused by, e.g., continuum shape differences.

(a) In order to account for differences in spectral resolution, we broadened the spectra with a Gaussian of wavelength-dependent width, such that the Lick/IDS resolution was best matched at each wavelength (see fig. 7 in WO97). After this step our spectra should resemble very well the general properties of the original spectra obtained by the Lick group.

(b) In a second step we need to correct the indices for velocity dispersion broadening. The observed spectrum of a galaxy is the convolution of the integrated spectrum of its stellar population(s) by the instrumental broadening and the distribution of line-of-sight velocities of the stars. These effects broaden the spectral features, in general reducing the observed line-strength compared to the intrinsic values. In order to compare the raw index measurements for galaxies with model predictions, we calibrate the indices to zero velocity dispersion. Spectra of 15 different G9–K4 giant stars were first broadened to the Lick/IDS resolution, and then further broadened using a Gaussian to $\sigma = 20$–$360\,\mathrm{km\,s^{-1}}$ in steps of $20\,\mathrm{km\,s^{-1}}$. The indices are then measured for each star and σ-bin and a correction factor, $C(\sigma)$, such that $C(\sigma) = \mathrm{Index}(0)/\mathrm{Index}(\sigma)$ is determined.

Fig. B2 in Appendix B shows the dependence of the correction factor on σ for all 16 indices. Note that for the molecular indices Mg_1 and Mg_2 and the index $H\gamma_F$[2] the correction factor is defined as $C(\sigma) = \mathrm{Index}(0) - \mathrm{Index}(\sigma)$. The scatter in $C(\sigma)$ at $360\,\mathrm{km\,s^{-1}}$ was <5 per cent for all indices but Hβ.

It is worth looking in detail why the Hβ velocity dispersion correction seems to be so insecure. The derived correction factors are useful only if the stars used for the simulations resemble the galaxy spectra. In principle, one might expect a dependence of the correction factor on line-strength – but most indices do not show such a behaviour. In fact, Hβ is the only index where we find a significant influence of line-strength on the correction factor at a given σ. It turns out that stars which exhibit Hβ absorption ≤ 1.1 Å lead to correction factors of $C(\sigma) < 1.0$, and stars with Hβ absorption >1.1 Å imply positive corrections. In the Fornax sample there are no galaxies with Hβ absorption line-strength of less than 1.4 Å; hence only stars with an Hβ index greater 1.1 Å have been used to evaluate the correction factor (scatter <5 per cent).

Another way to check the accuracy of the velocity dispersion corrections is to use galaxy spectra with small internal velocity dispersions as templates and treat them in the same way as stars. The galaxies NGC 1373, NGC 1380A, NGC 1336, IC 1963 and ESO 358-G59 were used for this purpose. They span a range in Hβ absorption of ~ 1.7–3 Å, and a range in central velocity dispersion of $\sigma_0 = 54$–$96\,\mathrm{km\,s^{-1}}$. In Fig. B2 the galaxies are represented by open circles, and they agree very well with the stellar correction for most of the indices. As expected for Hβ, the galaxies match the results from stars with an Hβ absorption >1.1 Å.

The final correction factors are derived by taking the mean of 15 stars and the five galaxies in each σ-bin (solid line in Fig. B2). The velocity dispersion corrections are applied by a `FORTRAN` program which reads in the raw index-measurements from continuum-corrected and resolution-corrected galaxy spectra. For each galaxy and index it applies a correction for velocity dispersion. The program linearly interpolates between σ-bins and also adds the error from the velocity dispersion correction factor to the raw Poisson error of the spectra. As the error in the correction factor is much bigger than any error caused by uncertainties in σ, we assumed the velocity dispersion of the galaxies to be error-free.

(c) Although we have matched very well the spectral resolution of the Lick system, small systematic offsets of the indices introduced by continuum shape differences are generally present (note that the original Lick/IDS spectra are not flux-calibrated). To establish these offsets, we compared our measurements for stars in common with the Lick/IDS stellar library. In total, we observed 13 different Lick/IDS stars. Fig. B1 in Appendix B shows the difference between Lick/IDS measurements and ours *after* the mean offset has been removed. The mean offsets and associated errors for each index are summarized in Table 4. The star HD 221148 was excluded from the offset analysis, because our index measurements proved to be very different from the original Lick/IDS measurements – possibly due to its variable nature (see Table 3). The formal error in the offset is evaluated by the mean standard deviation of stars with respect to the mean offset divided by $\sqrt{n_{\mathrm{stars}} - 1}$.

Most of the indices show small offsets to the Lick/IDS system, similar to the ones quoted in (WO97, table 9). The rather large offset in Mg_2 is due to a well-known difference in continuum shape.

Recently, Trager et al. (1998) published the Lick/IDS library of extragalactic objects including seven galaxies in the Fornax cluster and NGC 3379. We can check our previous offset evaluation by comparing our galaxy measurements with Trager et al. For this purpose we extracted a 3-pixel central aperture

Table 4. Lick/IDS offsets.

Index	offset (Lick/IDS–AAT)
G4300	$+0.21 \pm 0.09$ Å
Fe4383	$+0.60 \pm 0.13$ Å
Ca4455	$+0.37 \pm 0.06$ Å
Fe4531	$+0.00 \pm 0.10$ Å
$C_2$4668	-0.19 ± 0.17 Å
Hβ	-0.05 ± 0.04 Å
Fe5015	$+0.00 \pm 0.08$ Å
Mg_1	$+0.003 \pm 0.002$ mag
Mg_2	$+0.023 \pm 0.003$ mag
Mg b	$+0.15 \pm 0.09$ Å
Fe5270	$+0.07 \pm 0.05$ Å
Fe5335	$+0.00 \pm 0.08$ Å
Fe5406	$+0.00 \pm 0.04$ Å
Fe5709	$+0.00 \pm 0.06$ Å
$H\gamma_A$	$+0.45 \pm 0.28$ Å
$H\gamma_F$	$+0.00 \pm 0.14$ Å

[2] This index is actually not a molecular index, but typical index values are close to zero; hence a correction *factor* can degenerate.

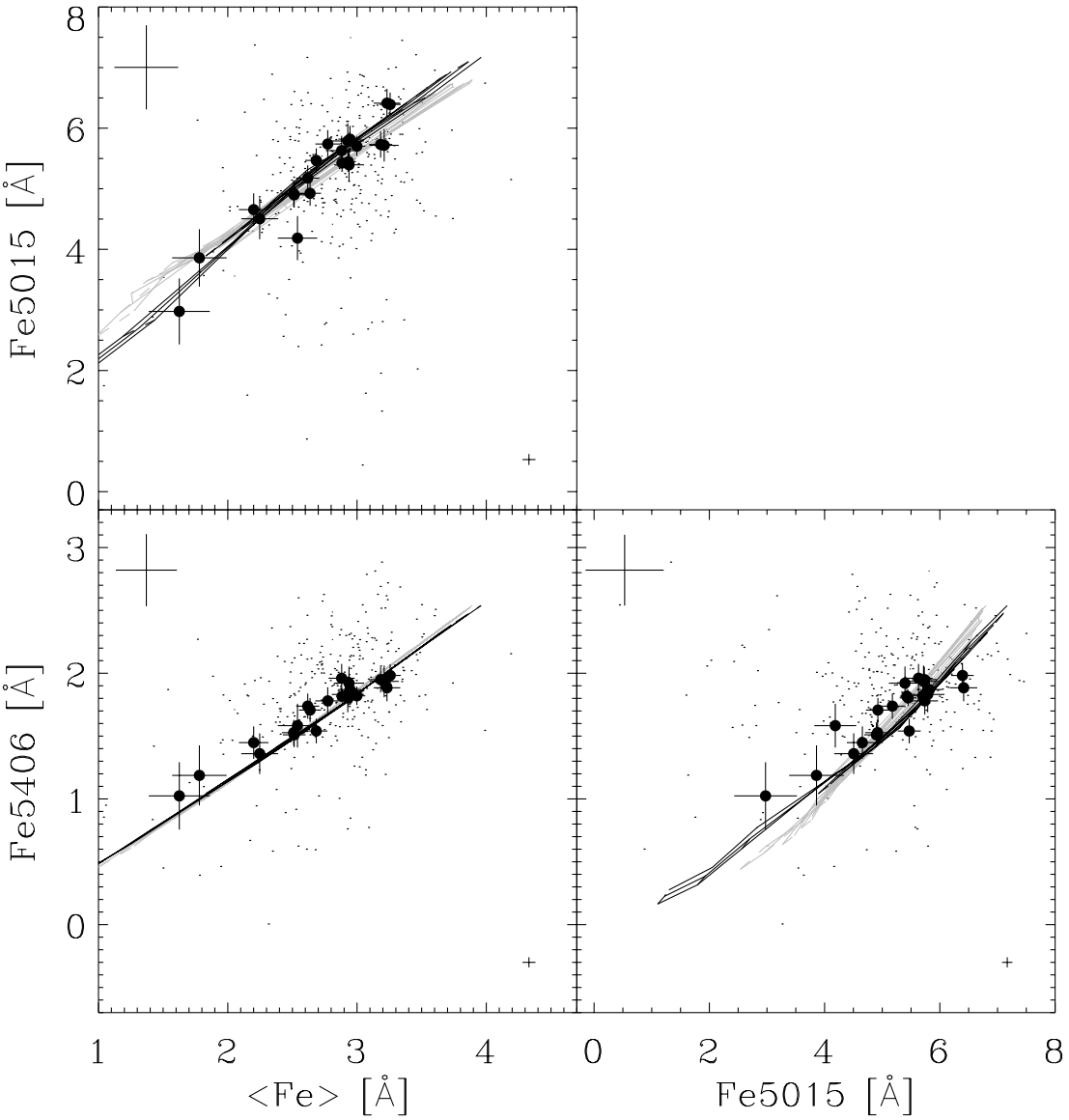

Figure 1. Index versus index plots for three well-established Fe-indicators in the Lick/IDS system. The filled circles and small dots represent AAT and Lick/IDS galaxy measurements respectively. The error bar in the upper left corner represents the average observational error for Lick/IDS galaxies, whereas for the AAT data the observational errors are shown for each individual galaxy. The error bar in the lower right corner shows the rms error in the offset to the Lick/IDS system for the AAT data. Overplotted are model predictions by Worthey (1994, black lines) and Vazdekis et al. (1996, grey lines). Note that Worthey models use a Salpeter IMF, whereas Vazdekis models use a bimodal IMF which is very similar to Salpeter for $M > 0.6\,M_{\odot}$.

($2.3 \times 2.44\,\mathrm{arcsec}^2$) for our galaxies matching the Lick/IDS standard aperture of $1.4 \times 4\,\mathrm{arcsec}^2$. Our indices are then corrected for velocity dispersion as described in paragraph (b), and the offsets from Table 4 are applied. The results are overplotted in Fig. B1 in Appendix B (filled symbols). The galaxies show for all indices more scatter around the mean offset than the stars which is somewhat reflected in the bigger error bars, but there are also some outliers. This is not surprising, as seeing effects and aperture differences will introduce some non-reproduceable offsets for individual galaxies. Furthermore, we note that the Lick group had to observe the Fornax galaxies at a very high airmass. With the possible exception of the indices G4300 and Fe4383, the offsets inferred from the galaxy comparison are consistent with the stellar comparison.

The offsets listed in Table 4 were applied to all indices after the correction for velocity dispersion. Note that the Lick/IDS-system offset-error is a constant value and does not depend on the velocity dispersion of the galaxy itself. Therefore we did not include this error in the individual index errors, but rather quote for each index a common offset error (see also Table 4). The final corrected central ($2.3 \times 3.85\,\mathrm{arcsec}^2$) index measurements and associated errors for the Fornax galaxies and NGC 3379 are presented in Table D2 in Appendix D. For each galaxy we give the index measurement in the first row and the 1σ error in the second row.

Note that for the galaxies NGC 1381 and NGC 1427 we combined three exposures yielding a very high S/N spectrum. Here our index-error estimation taking into account only the Poisson error becomes invalid because of other error sources such as the wavelength calibration, continuum correction and aperture effects. By comparing individual exposures we established that 1.5 times the original Poisson error estimate is a good indicator of the

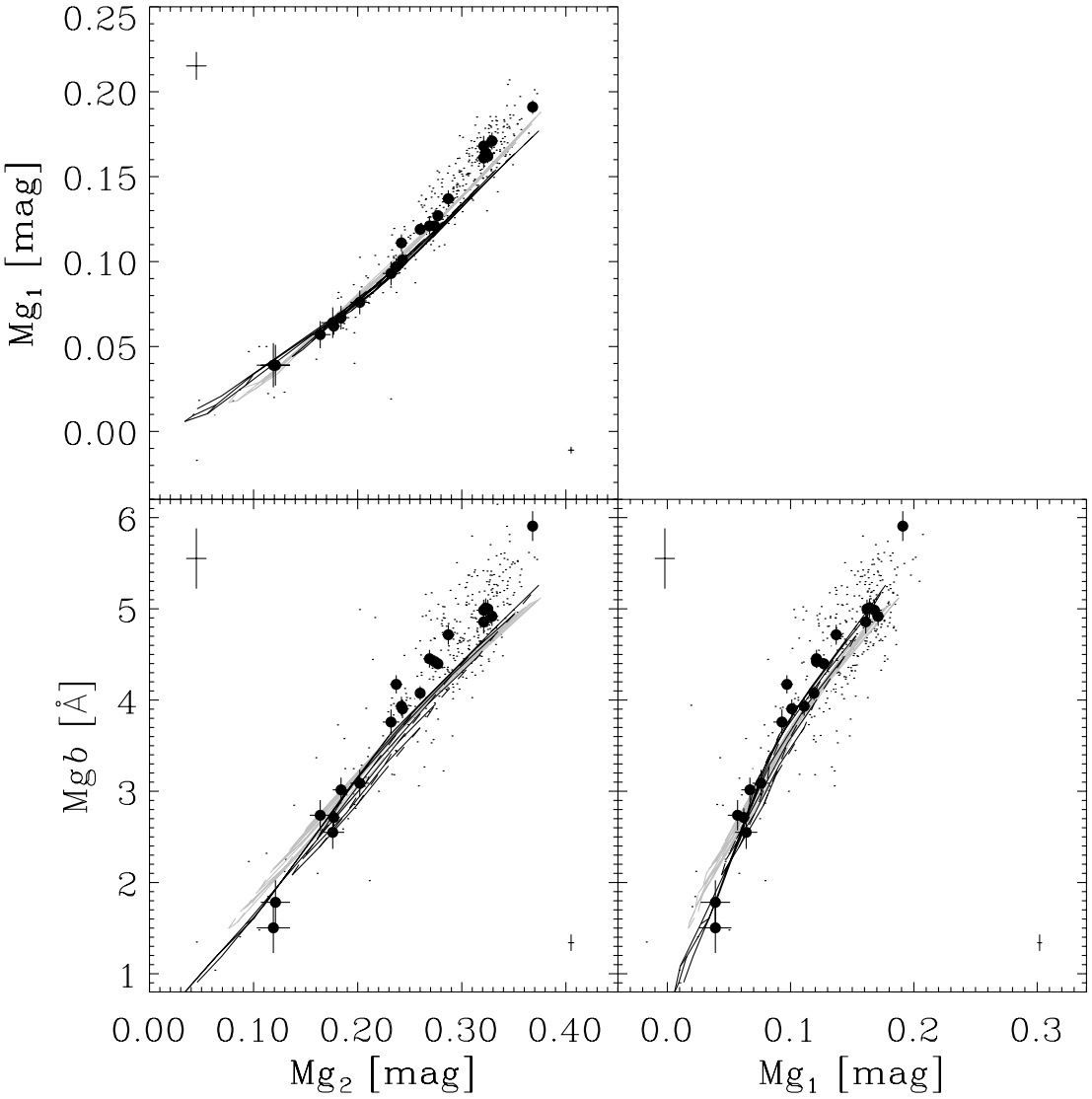

Figure 2. Index versus index plots for the three Mg indices in the Lick/IDS system. Overplotted are model predictions by Worthey (1994, black lines) and Vazdekis et al. (1996, grey lines).

true error. This adjusted error was adopted in Table D2 and for any further analysis.

4 A CONSISTENCY TEST OF THE MODEL PREDICTIONS

For the following analysis of the nuclear stellar populations (Section 5) it is extremely important that our index measurements are accurately calibrated on to the Lick/IDS system, which is based on the Lick/IDS stellar library (Worthey et al. 1994). Here we investigate the accuracy and consistency of our calibration and the model predictions by presenting index–index plots which are almost degenerate in age and metallicity. In that way the model predictions cover only a small 'band' of the parameter space, and they should trace the relation of the galaxies if the models describe accurately the galaxy properties and our calibration is accurate. Fig. 1 shows the relation between $\langle$Fe$\rangle$,[3] Fe5015 and Fe5406 for our sample of galaxies (filled circles) and the original Lick/IDS sample of galaxies (Trager et al. 1998, small dots). Overplotted are models by W94 (black lines) and V96 (grey lines). The plots show a good agreement between index measurements and the model predictions. The reduced Poisson noise of our data set compared to the Lick/IDS measurements can be clearly seen (see also figure caption). We note that the model predictions of W94 and V96 are in good agreement.

A similar analysis of the three Mg indices is shown in Fig. 2. Here we find a significant deviation of the measured index values compared to the model predictions for metal-rich and/or old stellar populations. The deviations are seen in the Fornax sample as well as in the original Lick/IDS galaxy spectra (see also Worthey 1992, figs 5.12 and 5.13). We therefore note that this discrepancy is inherent to the Lick/IDS system and models, and any models which use the Lick/IDS fitting functions are likely to show the same offset. In Fig. 3 we present the Balmer indices Hβ, H$\gamma_{\rm A}$ and H$\gamma_{\rm F}$. Here we find generally good agreement with small deviations between model predictions and data at low values of H$\gamma_{\rm A}$ versus H$\gamma_{\rm F}$ which are present in our data and the original Lick/IDS measurements.

[3] $\langle$Fe$\rangle$ = (Fe5270 + Fe5335)/2.

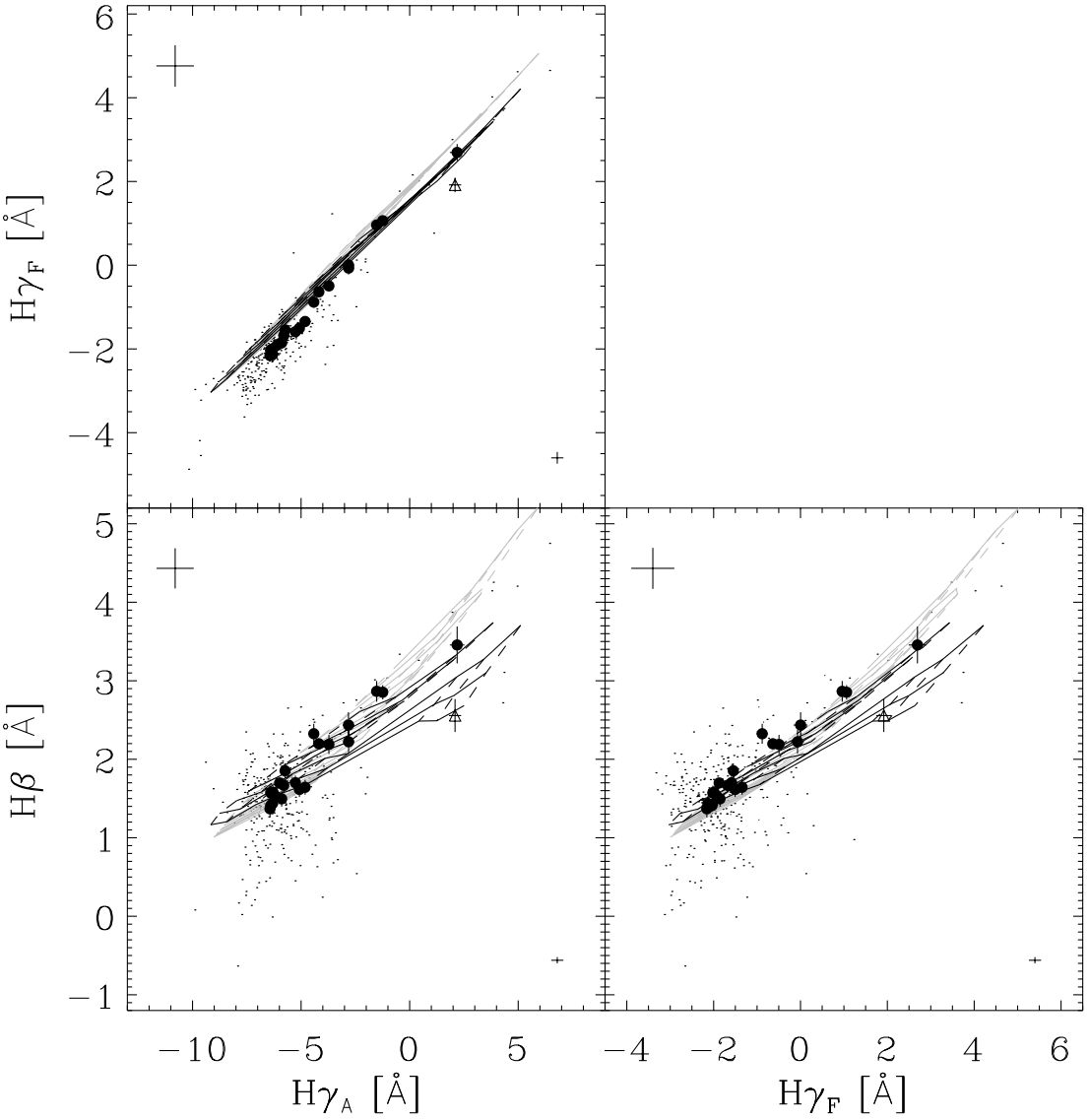

Figure 3. Index versus index plots for three Balmer line indices in the Lick/IDS system. Symbol definitions are the same as in Fig. 1, except for the galaxy ESO 358-G25 which is represented by an open triangle. This galaxy is affected by emission in the Balmer lines. Overplotted are model predictions by Worthey (1994, black lines), Worthey & Ottaviani (1997, black lines) and Vazdekis et al. (1996, grey lines).

Figs 1 to 3 suggest that our Lick/IDS calibration is very consistent with the original galaxy measurements of the Lick group. However, we note that small, systematic offsets exist between the parameter space covered by galaxies and the model predictions for magnesium at high index values and for Balmer lines at low index values.

5 THE NUCLEAR STELLAR POPULATIONS

The aim of this section is to derive estimates of the mean (luminosity-weighted) ages and metal abundances of early-type galaxies in the Fornax cluster. As pointed out by W94, the determination of the ages and metallicities of old stellar populations is complicated by the similar effects that age and metallicity have on the integrated SEDs. However, this degeneracy can be partially broken by plotting a particular age-sensitive index, such as one of the Balmer line indices, against a more metallicity-sensitive index. The usefulness of this approach has been demonstrated by many authors (González 1993; Fisher et al. 1995; Kuntschner & Davies 1998; Mehlert 1998; Jørgensen 1999). However, as we will see in this section, among other issues the treatment of non-solar abundance ratios is a crucial parameter in the determination of absolute age and metallicity estimates. We will also investigate the effects of nebular emission and composite stellar populations on age/metallicity estimates in Sections 5.2 and 5.3 respectively, before we present our best age/metallicity estimates of the Fornax early-type galaxies in Section 5.4.

5.1 Non-solar abundance ratios

In Fig. 4 we present age/metallicity diagnostic diagrams of six metallicity-sensitive indices (Mg_2, $C_2$4668, Ca4455, Fe3, $\langle$Fe$\rangle$ and Fe5406) plotted against the age-sensitive Balmer line indices Hβ and Hγ_A (the new index Fe3 is defined in equation 1). Fig. 4(h) is a reproduction from Kuntschner & Davies (1998) with minor data up-dates. Overplotted are model predictions from W94, WO97

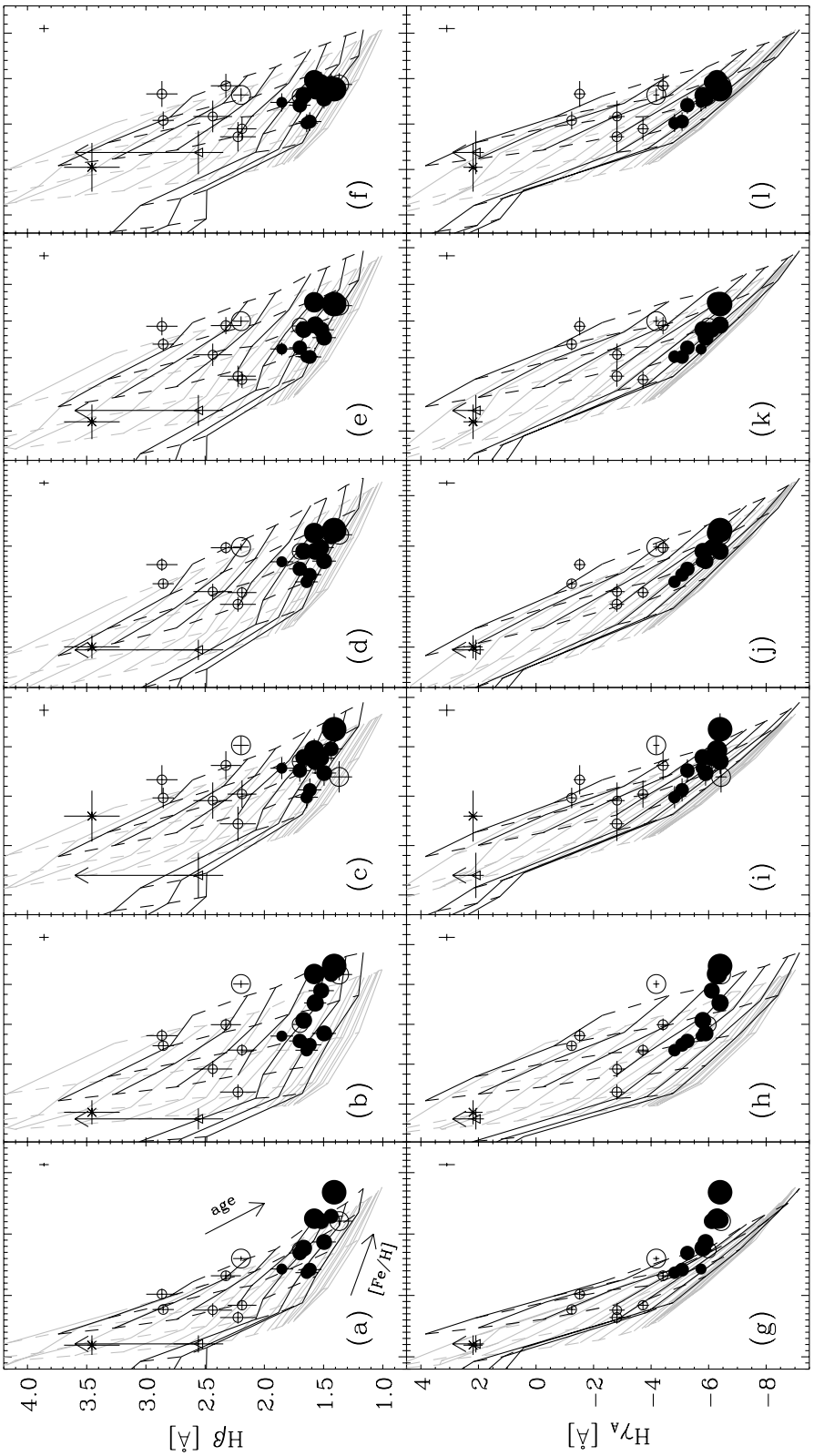

Figure 4. The two age-sensitive indices Hβ and Hγ_A plotted against six metallicity indicators: Mg_2, $C_2$4668, Ca4455, Fe3, ⟨Fe⟩ and Fe5406. Models by Worthey (1994, black lines), Worthey & Ottaviani (1997, black lines) and Vazdekis et al. (1996, grey lines) are overplotted. The solid lines represent isoage lines, whereas the dashed lines are lines of constant metallicity. Filled circles and open circles represent ellipticals and S0s respectively. The star and open triangle represent possible post-starburst and starburst galaxies respectively. The arrow attached to ESO 358-G25 (open triangle) indicates an emission correction. The symbol size is scaled with the central velocity dispersion of the galaxies. The cross in the upper right corner of each panel indicates the rms uncertainty in the transformation to the Lick/IDS system. Observational errors are plotted as individual error bars on the data points.

(black lines) and V96 (grey lines). The solid lines represent lines of constant age, and the dashed lines are lines of constant metallicity. The Worthey models span ranges in age of 1.5–5 Gyr with [Fe/H] = −0.225 to 0.5, and 8–17 Gyr with [Fe/H] = −2 to 0.5. The V96 models span a range in age of 1–17.4 Gyr with [Fe/H] = −0.7 to 0.4. The direction of increasing age and metallicity is indicated in Fig. 4(a) by arrows.

Our previous result from Kuntschner & Davies (1998), namely that Fornax ellipticals form a sequence in metallicity at high ages and that the S0s spread to lower ages, is confirmed in all diagrams. Examining the diagrams in detail, one can see that the mean age and metallicity of the sample changes from diagram to diagram; e.g., the ellipticals appear older and more metal-poor in the ⟨Fe⟩ versus $H\gamma_A$ diagrams compared to the Mg_2 versus $H\gamma_A$ diagram. This effect was previously reported and recently reviewed by Worthey (1998). It is now widely accepted that this discrepancy in the model predictions is caused by non-solar abundance ratio effects. For example, Mg as measured by the Mg_2 index is overabundant compared to Fe in luminous elliptical galaxies, i.e., [Mg/Fe] > 0 (O'Connell 1976; Peletier 1989; Worthey et al. 1992; Davies et al. 1993; Weiss et al. 1995; Jørgensen 1997, 1999).

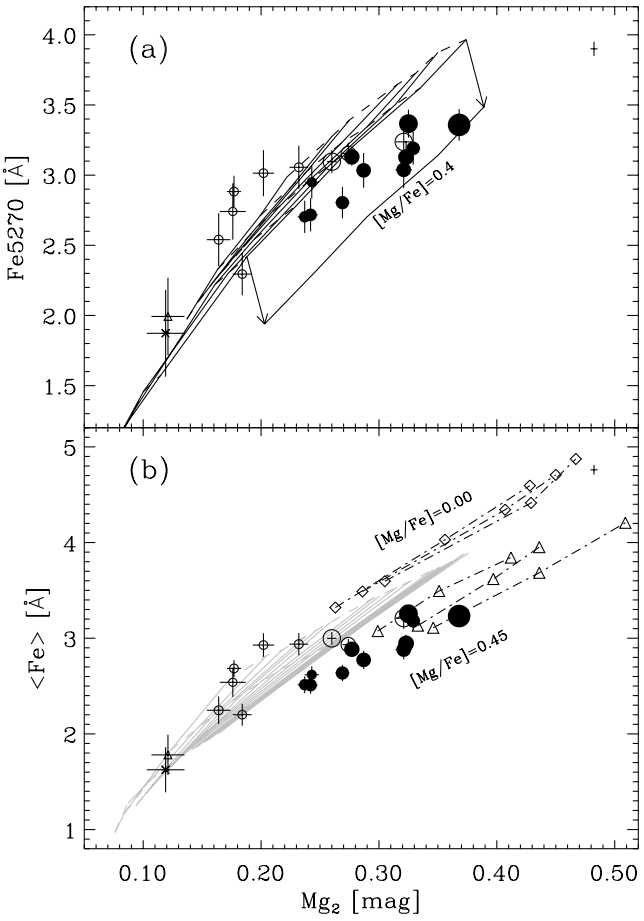

Figure 5. (a) Mg_2 versus Fe5270 equivalent width diagram for the complete sample of Fornax early-type galaxies. Overplotted are models by Worthey (1994) and a correction for [Mg/Fe] = 0.4 for the 17 Gyr isoage line (taken from Greggio 1997). (b) Mg_2 versus ⟨Fe⟩ diagram. Overplotted are models by Vazdekis et al. (1996, grey lines) and two models by Weiss, Peletier & Matteucci (1995, dot-dashed lines). The Weiss et al. models are calculated for three ages, 12, 15 and 18 Gyr (dot-dashed lines represent lines of constant age) at $Z = 0.02$, 0.04 and 0.07, a mixing length parameter $\alpha_{MLT} = 1.5$, and somewhat different mixes of heavy elements. Steps in metallicity are shown as diamonds for [Mg/Fe] = 0.0 and as triangles for [Mg/Fe] = 0.45. Symbol definitions as in Fig. 4.

The Mg overabundance can be examined in a Mg-index versus Fe-index plot (Worthey et al. 1992). In such a diagram the model predictions cover only a narrow band in the parameter space, as effects of age and metallicity are degenerate. Fig. 5 shows plots of ⟨Fe⟩ and Fe5270 versus Mg_2 for the Fornax sample. Overplotted are model predictions from W94, V96 and Weiss et al. (1995). We assume that the models reflect solar abundance ratios if not stated otherwise, i.e., [Mg/Fe] = 0. If the model predictions accurately resemble the galaxy properties, they should trace the observed relation. The measured line-strength of most of the S0s agrees with the model predictions, perhaps 3–4 galaxies having slightly low Mg_2 absorption compared to Fe5270 and ⟨Fe⟩. However, for most of the ellipticals and the S0 NGC 1380, the models predict too little Mg-absorption at a given Fe absorption strength. Additionally, the most metal-rich galaxies are the furthest away from the model grids. Using the Mg overabundance correction by Greggio (1997, see Fig. 5a) and the models for [Mg/Fe] = 0.45 by Weiss et al. (1995), we conclude that the stellar populations of Fornax ellipticals and the bulge of NGC 1380 are Mg-overabundant relative compared to Fe. The overabundance ranges between [Mg/Fe] = 0.0 and ∼0.4. We note that there is a considerable spread in overabundance at a given Fe-line strength in our sample.

Non-solar abundance ratios do exist not only in elliptical galaxies but also in our own Galaxy where stars show an overabundance for α-elements[4] at [Fe/H] $\lesssim 0.0$ (Edvardsson et al. 1993; McWilliam 1997). Of course, if those stars are incorporated in a stellar library which in turn is used for model predictions of integrated stellar populations, the predictions will be somewhat α-element-overabundant at low metallicities. We therefore note that models which use the Lick/IDS fitting functions are probably α-element-overabundant at low metallicities, which makes it more difficult to interpret trends in diagrams such as Fig. 5.

Several indices covered by our wavelength range show deviations from the model predictions when compared to the average Fe index: Mg_1, Mg_2, Mg *b*, Fe5709 and $C_2$4668. Fe5709 is a very weak index, and its correction for velocity dispersion broadening may well be insecure, so we cannot draw any firm conclusions. $C_2$4668 is an important index, because it shows the strongest total metallicity sensitivity in the Lick/IDS system (Worthey 1998) and is therefore preferentially used in age/metallicity diagnostic diagrams. In Fig. 6 we present a plot of $C_2$4668 versus Fe3. Fe3 is a combination of three prominent Fe lines, thus maximizing its sensitivity to Fe while minimizing the Poisson errors:

$$\mathrm{Fe3} = \frac{\mathrm{Fe4383} + \mathrm{Fe5270} + \mathrm{Fe5335}}{3}. \quad (1)$$

As a consequence of the extreme metallicity sensitivity of $C_2$4668, the models are not as degenerate as in the previous plots. Nevertheless, it is clear that for a $C_2$4668 absorption strength in excess of ∼6 Å the model predictions do not follow the observed trend (see also Kuntschner 1998). Hence we conclude that $C_2$4668, or better at least one of the species contributing to the index, is overabundant compared to Fe in metal-rich Fornax galaxies. Can this overabundance be caused by Mg as seen in the Fe versus Mg plot (Fig. 5)? Due to the proximity of metal

[4] α includes the elements O, Mg, Si, S, Ca and Ti.

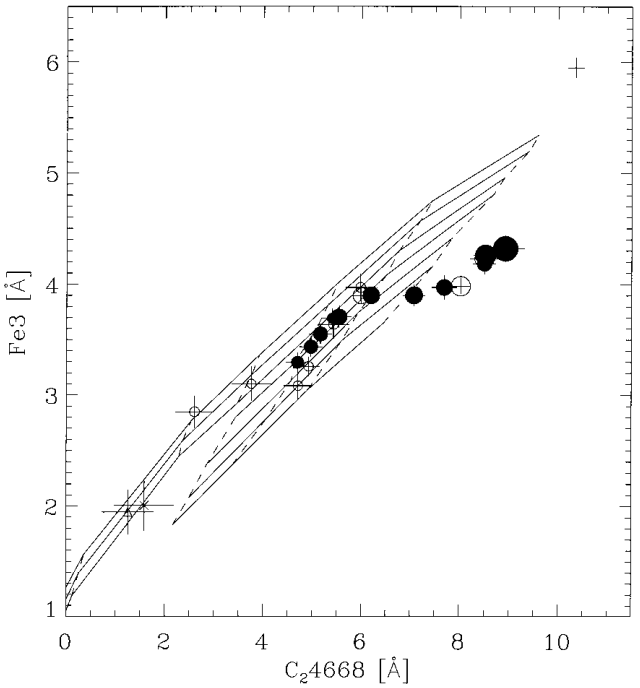

Figure 6. $C_2$4668 equivalent width versus Fe3 equivalent width. Overplotted are models by Worthey (1994). The $C_2$4668 index shows evidence of overabundance compared to Fe3 at strong absorption strength (>6.5 Å). The symbol size is scaled with the central velocity dispersion of the galaxies.

absorption lines in the optical wavelength region none of the Lick/IDS indices measures the abundance of only a particular element such as Fe or Mg. There are always contributions from other elements or molecules to an index (Tripicco & Bell 1995). In particular, the $C_2$4668 index has a relatively wide central bandpass (86.25 Å), including a wide range of metal lines. The most dominant species here is carbon in the form of C_2-bands which blanket the central bandpass (Tripicco & Bell 1995). However, more important here is the fact that according to Tripicco & Bell (1995; table 6, cool giants) the $C_2$4668 index *decreases* when the Mg abundance (or oxygen abundance) is *increased* (at fixed abundances of all other elements). Therefore the 'overabundance' of $C_2$4668 cannot be caused by Mg. What exactly drives the overabundance of $C_2$4668 compared to Fe remains to be seen.

The overabundance of certain elements compared to Fe has a profound effect on the use of age/metallicity diagnostic diagrams if the model predictions reflect only solar abundance ratios. Recalling Fig. 4(h) (see also Kuntschner & Davies 1998), we find that not only are the metallicities (measured as [Fe/H]) over-estimated due to the $C_2$4668 overabundance, but furthermore much of the age upturn at high metallicities is caused by the overabundance. The effect of changing the age estimates is caused by the residual age/metallicity degeneracy which is still present in all diagrams in Fig. 4. Only if the index-combination breaks the degeneracy completely, i.e., if lines of constant age and constant metallicity are perpendicular, would the age estimates not be affected by non-solar abundance ratios. We further note that trends in abundance ratios within a data set such as our Fornax sample (increasing Mg/Fe with galaxy mass) can lead to artificial relative age trends in diagrams such as that in Fig. 4(h). Taking into account not only the uncertainties introduced by non-solar abundance ratios but also other model parameters such as which isochrone library to use, it seems very insecure to derive *absolute* age estimates from the currently available stellar population models.

Introducing non-solar abundance ratios in model predictions is rather complicated, as accurate model predictions do need a stellar library covering the whole parameter space of T_e, $\log g$, [Fe/H] *and* [Mg/Fe]. Furthermore, new isochrone calculations may well be needed for each [Mg/Fe] bin: recently, Salaris & Weiss (1998) suggested that scaled-solar isochrones cannot be used to replace Mg-enhanced ones at the same total metallicity. The latter will not only change the model predictions for indices such as Mg_2, but may affect all indices and in particular the age-sensitive ones such as Hβ and Hγ_A (see also Worthey 1998). However, note that Weiss et al. (1995) concluded in their study that scaled solar isochrones are sufficient to calculate model predictions for non-solar abundance ratios.

Another way to examine non-solar abundance ratios is to compare the metallicity estimates derived from different metal lines using the same age indicator. Fig. 7 compares the metallicity estimates taken from Mg_2, $C_2$4668, Fe5406 and Ca4455 versus Hβ diagrams with the estimates taken from a Fe3 versus Hβ diagram. Here Fe3 serves as our mean Fe-abundance indicator. The metallicity estimates are derived from the V96 models.[5] To get more accurate estimates, the age/metallicity–grid was expanded to a step size of 0.025 in [Fe/H] by linear interpolation. Furthermore, the diagram was extrapolated to [Fe/H] = +0.7 by linear extrapolation. The age range of 1 to 17.4 Gyr is covered by 18 grid points. Errors on the metallicity estimates were derived by adding and subtracting the index error for each galaxy individually (Poisson error and Lick/IDS offset error added in quadrature) and re-deriving the metallicity estimates. The final uncertainty displayed in Fig. 7 was taken to be 0.7 times the maximum change in [Fe/H].

In panel (a) of Fig. 7 we can clearly see that for elliptical galaxies Mg_2 gives metallicity estimates which are larger than those derived from Fe3, and there is a trend that the Mg overabundance increases with increasing metallicity. Most of the S0s are consistent with solar or slightly less than solar abundance ratios of Mg/Fe. However, the (more luminous) S0s NGC 1380 and 1381 show a weak overabundance of Mg. The index $C_2$4668 (panel b) gives on average high metallicity estimates compared to Fe3. Although three galaxies with just above solar metallicity show solar abundance ratios. As expected, the Fe index Fe5406 (panel c) is in good agreement with the estimates derived from Fe3. The Ca4455 index (panel d) gives marginally higher metallicity estimates compared to the Fe3 indicator. We note that the Ca4455 index is more sensitive to a mix of heavy elements than to calcium on its own, despite its name (Tripicco & Bell 1995).

In conclusion, we can confirm our previous results that Mg and $C_2$4668 are overabundant compared to Fe. The Mg overabundance follows a trend where metal-rich (and luminous) Es show a stronger overabundance than less luminous and metal-poor galaxies.

[5] These models have a bimodal IMF which is very similar to the Salpeter IMF for $M > 0.6\,M_\odot$. Note that for an age of ~17 Gyr, V96 models predict 0.1–0.2 Å less Hβ absorption compared to W94 models. This, of course, will affect the absolute age estimates, but it has little affect on the metallicity estimates.

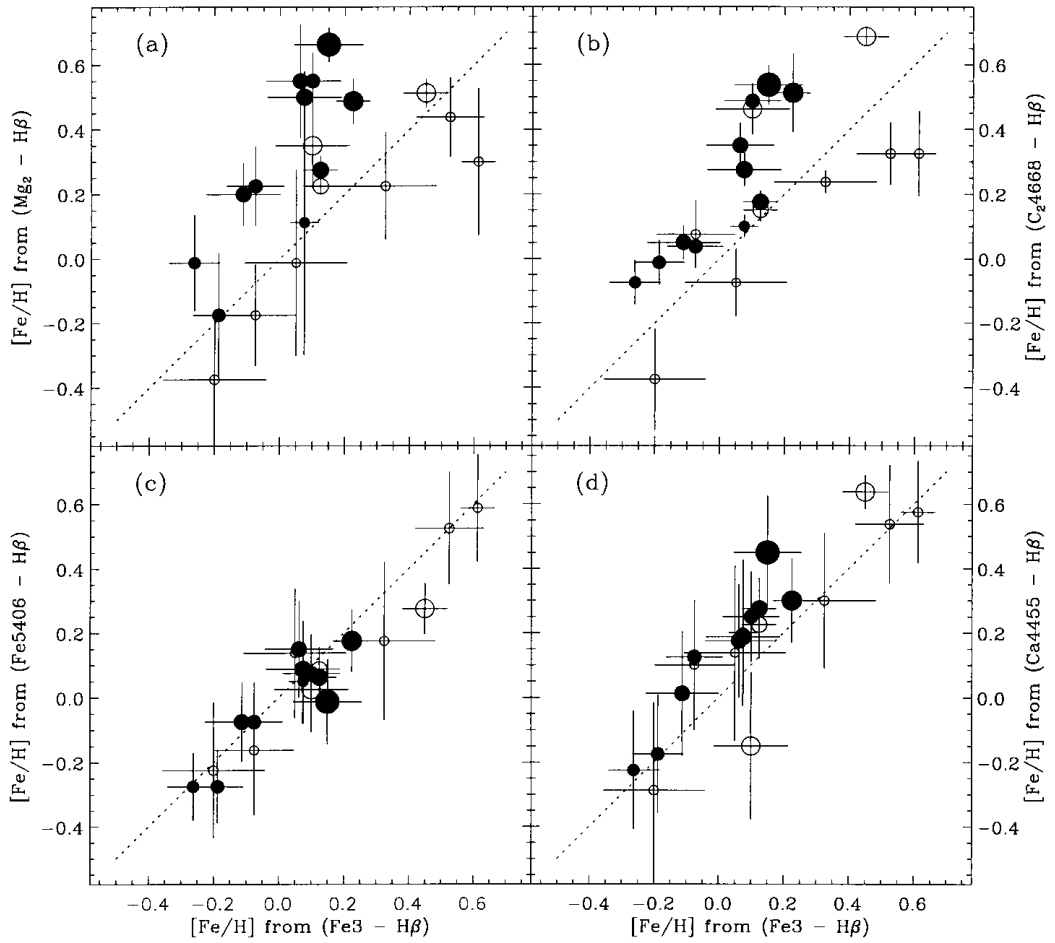

Figure 7. Metallicity estimates derived from four age–metallicity diagnostic diagrams, all using Hβ as age indicator but different metal lines (Mg_2, Fe5406, $C_2$4668 and Ca4455), are compared with the metallicity estimates from the Fe3 versus Hβ diagram. The filled circles represent elliptical galaxies, and the open circles stand for the S0s. The symbol size is scaled with the central velocity dispersion of the galaxies.

5.2 Nebular emission in early-type galaxies

So far we have concentrated on breaking the age/metallicity degeneracy and the treatment of non-solar abundance ratios. A further important issue when estimating ages and metallicities from line-strength indices is nebular emission. Elliptical galaxies normally contain much less dust and ionized gas than spirals; in fact, for a long time they were regarded as dust- and gas-free. However, spectroscopic surveys of large samples of early-type galaxies revealed that about 50–60 per cent of the galaxies show weak optical emission lines (Caldwell 1984; Phillips et al. 1986). Typically, the reported strength of emission lines such as [O II], [Hα] and [N II] λ6584 indicates the presence of only 10^3–10^5 $M_\odot$ of warm ionized gas in the centre. A more recent study of 56 bright elliptical galaxies by Goudfrooij et al. (1994) detected ionized gas in 57 per cent of their sample and confirmed the amount of ionized gas present. Additionally, *HST* images of nearby bright early-type galaxies revealed that approximately 70–80 per cent show dust features in the nucleus (van Dokkum & Franx 1995). Stellar absorption-line-strength measurements can be severely affected if there is emission present in the galaxy which weakens the stellar absorption (Goudfrooij & Emsellem 1996). For example, nebular Hβ emission on top of the integrated stellar Hβ absorption weakens the Hβ-index and leads therefore to wrong, i.e., too high age estimates.

The spectrum of ESO 358-G25 shows clear emission in Hβ and Hγ along with weak [O III] emission (see Kuntschner & Davies 1998, fig. 3). As a consequence, the age is overestimated in Figs 4(a)–(f). The arrow attached to ESO 358-G25 indicates a rough emission correction. However, it is extremely difficult to accurately correct the Hβ-index in individual galaxies for emission contamination. A much better method to reduce emission contamination is to use higher order Balmer lines such as Hγ, as they are less affected by nebular emission (Osterbrock 1989). Indeed, in Figs 4(g)–(l) the galaxy ESO 358-G25 moves to much lower ages. As none of the other galaxies move significantly to lower ages, we conclude that nebular emission is not very prominent in our Fornax sample. This is supported by the absence of strong [O III]λ5007 emission. Only five galaxies show emission above our detection limit of $\sim$0.2 Å. The strongest emission is detected in ESO 358-G25 with 0.7-Å equivalent width (for details see Kuntschner 1998).

5.3 Effects of composite stellar populations

Most of the S0s in our sample have luminosity-weighted young stellar populations, with some of them also having high metallicities when compared to single-burst stellar population (SSP) models. However, these galaxies show only a central young stellar population on top of an underlying older one as opposed to

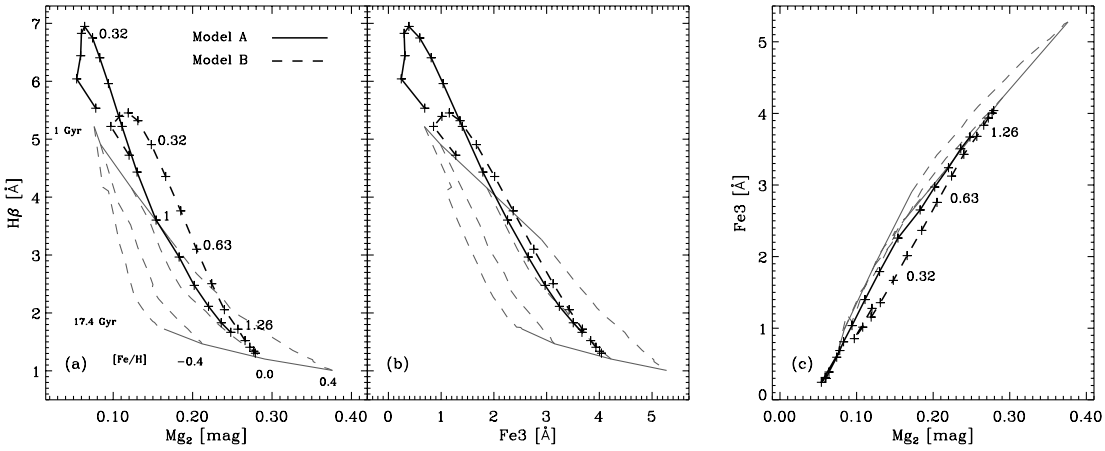

Figure 8. Evolutionary tracks based on Vazdekis et al. (1996) are shown in three index–index diagrams for a composite (Model A) of a 15 Gyr old (solar metallicity, 90 per cent mass) and a young stellar population (solar metallicity, 10 per cent mass) at burst ages 0.1, 0.13, 0.16, 0.2, 0.25, 0.32, 0.4, 0.5, 0.63, 0.79, 1.0, 1.26, 1.58, 2.0, 2.51 and 3.16 Gyr. The plus symbols along the tracks indicate the time-steps. Age-steps of 0.32 and 1 Gyr are also indicated by numbers in panel (a). Model B represents a burst of 1 per cent (in mass) strength with the same metallicities and age-steps as in Model A. Age-steps of 0.32, 0.63 and 1.26 Gyr are indicated in panel (a) and (c). The region of normal SSP models (Vazdekis et al. 1996) is shown as thin lines.

be entirely young. It is not straightforward to compare *composite* stellar populations with SSP models (de Jong & Davies 1997). So, how reliable are the age, metallicity and abundance ratio estimates taken directly from SSP models for these young galaxies? In order to explore this issue, we calculated model predictions based on V96 for simple composite stellar populations. Two representative tracks are shown in Fig. 8 for two age/metallicity diagnostic diagrams and a plot of Fe3 versus Mg_2 in order to explore the behaviour of abundance ratios: Model A is a 15-Gyr-old (90 per cent in mass) stellar population plus a burst (10 per cent in mass) of varying ages from 0.1 to ∼3 Gyr. Both populations have solar metallicity. For Model B we reduced the burst fraction to 1 per cent (in mass), while the other parameters are the same as in Model A.

Overall one can see in the age/metallicity diagnostic diagrams that for a short time the burst population will dominate the integrated light, leading to strong Hβ absorption and weak metal-line absorption. Then the underlying old population becomes more and more important, and after ∼3 Gyr the galaxy is almost back to its original place in the diagram. However, the burst strength influences the exact track which the galaxy takes in the diagram. For a burst of 10 or 20 per cent (not shown) in mass the tracks follow roughly the solar-metallicity line in the normal SSP models. However, for a small burst (1 per cent in mass) the integrated light looks for a short while as having metallicities well above solar. This effect is more pronounced for Mg_2 than for Fe3. Of course, this in turn leads to an artificially created over-abundance when these galaxies are compared to SSP models (see Fig. 8c). For bursts stronger than a few per cent the abundance ratios are not significantly affected.

In summary, we find that composite stellar populations and in particular small (in mass) bursts, such as used in our simple models, can lead to an overestimation of the metallicity in the context of SSP models. Abundance ratios can be affected in the sense that the Mg/Fe ratio is too high. Our model calculations show that these conclusions hold qualitatively if the metallicity is changed or different metallicities are combined. A more thorough investigation of these issues would be very valuable but is beyond the scope of this paper (see Hau, Carter & Balcells 1999 for a more detailed analysis).

5.4 Best age and metallicity estimates

Having examined some of the fundamental problems by applying stellar population model predictions to observed line-strength indices, we present in Fig. 9 what we consider our best age/metallicity diagnostic diagram. A mean Fe index (Fe3) is plotted against an emission-robust higher order Balmer line ($H\gamma_A$). Due to the lack of model predictions with non-solar abundance ratios we decided to avoid indices which are affected by overabundance problems (e.g., Mg and $C_2$4668). Instead, we use here a combination of Fe indices (Fe3) as a metal indicator which will bias our results towards the Fe abundance. We note, however, that our metallicities are not to be understood as total metallicity, but rather as a good estimate of the Fe abundance. Any non-solar abundance ratios which affect $H\gamma_A$ are ignored. Model predictions by W94 and V96 are overplotted in Fig. 9.

The ellipticals form a sequence of metallicity at roughly constant age. The centres of the bright S0s NGC 1380 and NGC 1381 follow the sequence of Es. The remaining S0s cover a large range in metallicity and spread to much lower luminosity-weighted ages than the Es. We emphasize that these age and metallicity estimates are *central luminosity-weighted* estimates, and for apparently young galaxies the derived parameters are somewhat more insecure (see previous discussion about the effects of composite stellar populations). The age and metallicity gradients within the galaxies will be discussed in a future paper. Fornax A, a bright peculiar S0, shows strong Balmer lines and strong Fe absorption, which translates into a luminosity-weighted young and metal-rich stellar population. As we will see in the next section, all other young or metal-poor S0s have velocity dispersions of $\sigma_0 \lesssim 70\,\mathrm{km\,s^{-1}}$. The two galaxies with the weakest metal lines and strong Hβ and $H\gamma_A$ absorption (ESO 359-G02, cross, and ESO 358-G25, open triangle) appear to be different from the rest of the sample. These galaxies are likely to be post-starburst or starburst galaxies respectively. They have remarkable spectra for early-type galaxies, showing blue continua, strong Balmer lines, and weak metal lines. These galaxies are amongst the faintest in our sample and are ∼3° away from the centre of the cluster (see also Kuntschner & Davies 1998).

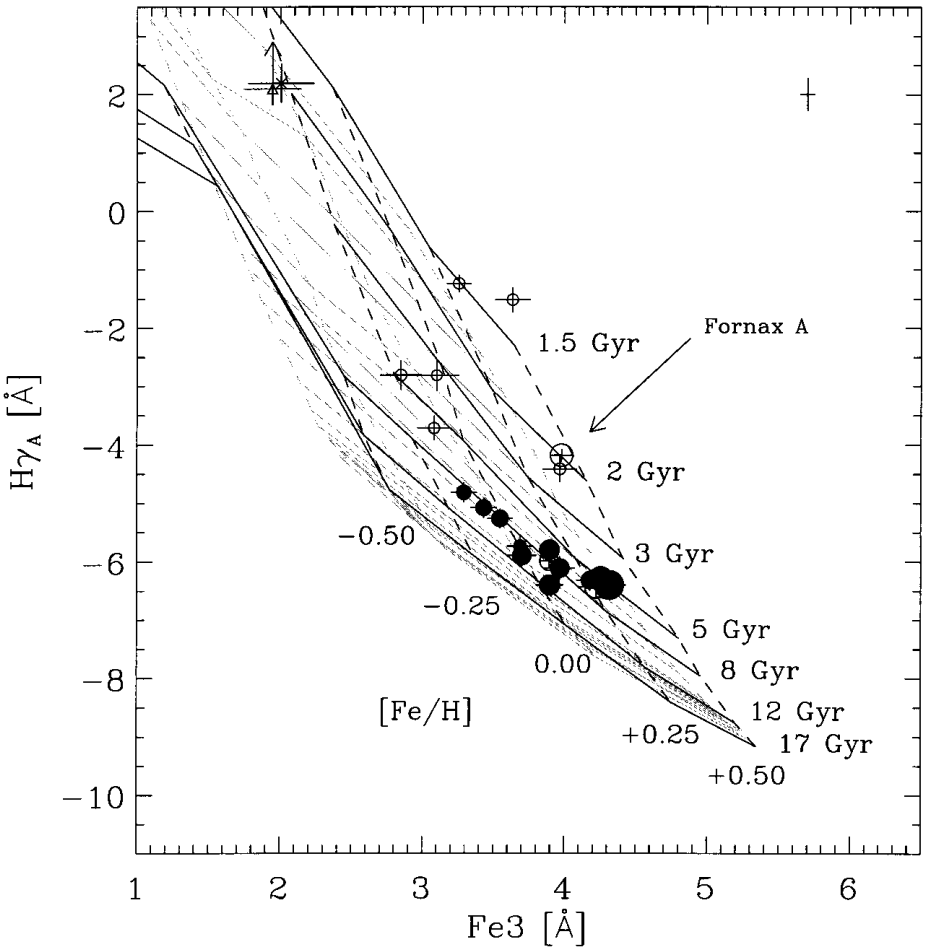

Figure 9. Fe3 equivalent width versus $H\gamma_A$ equivalent width. Filled circles and open circles represent ellipticals and S0s respectively. The star and open triangle represent possible post-starburst and starburst galaxies respectively. The cross in the upper right corner of each panel indicates the rms uncertainty in the transformation to the Lick/IDS system. The symbol size is scaled with the central velocity dispersion of the galaxies. Note that the two bright S0s are somewhat hidden in the sequence of Es.

6 LINE–STRENGTH INDICES AND THE CENTRAL VELOCITY DISPERSION

The central velocity dispersion σ_0 of early-type galaxies is known to correlate strongly with colours (Bower et al. 1992) and the absorption strength of the Mg-absorption feature at 5174 Å (Terlevich et al. 1981; Burstein et al. 1988; Bender, Burstein & Faber 1993; Jørgensen 1997; Colless et al. 1999). The relatively small scatter about these relations imply that the dynamical properties of galaxy cores are closely connected with their stellar populations. However, analysing the Mg–σ_0 relation for a sample of 736 mostly early-type galaxies in 84 clusters, the EFAR group (Colless et al. 1999) finds rather large dispersions in age (40 per cent) and in metallicity (50 per cent) at fixed velocity dispersion using the constraints from the Mg–σ_0 relation *and* the Fundamental Plane. Correlations of other metal indices, such as ⟨Fe⟩, with the central velocity dispersion have long been expected, but so far relations have shown a large scatter and only weak correlations (Fisher et al. 1996; Jørgensen 1997, 1999). However, we will demonstrate that galaxies in the Fornax cluster do show a clear correlation between Fe indices and central velocity dispersion.

Following Colless et al. (1999), we find it more convenient to express the 'atomic' indices in magnitudes like the 'molecular' index Mg_2. The new index is denoted by the index name followed by a prime sign [′], e.g., Mg b'. Note that by using only the logarithm of the atomic index, one introduces a non-linear term in comparison to the magnitude definition. Furthermore, negative index values such as for the $H\gamma_A$ index cannot be put on a simple logarithmic scale. A priori it is not clear whether log index or index′ correlates better with $\log\sigma_0$, but as the classical Mg–σ_0 relation was established with Mg_2 measured in mag, we adopt this approach here for all other indices as well. The conversion between an index measured in Å and magnitudes is

$$\text{index}' = -2.5\log\left(1 - \frac{\text{index}}{\Delta\lambda}\right), \tag{2}$$

where $\Delta\lambda$ is the width of the index bandpass (see, e.g., WO97 and Trager et al. 1998 for a list of bandpass definitions). Fe3′ is defined as

$$\text{Fe3}' = \frac{\text{Fe4383}' + \text{Fe5270}' + \text{Fe5335}'}{3}. \tag{3}$$

Fig. 10 shows index–σ_0 relations for eight different metal indices and two Balmer-line indices. The best-fitting linear relations and the scatter are summarized in Table 5 for all indices considered in this paper. For the fits we used an ordinary least-squares method, minimizing the residuals in y-direction (Isobe

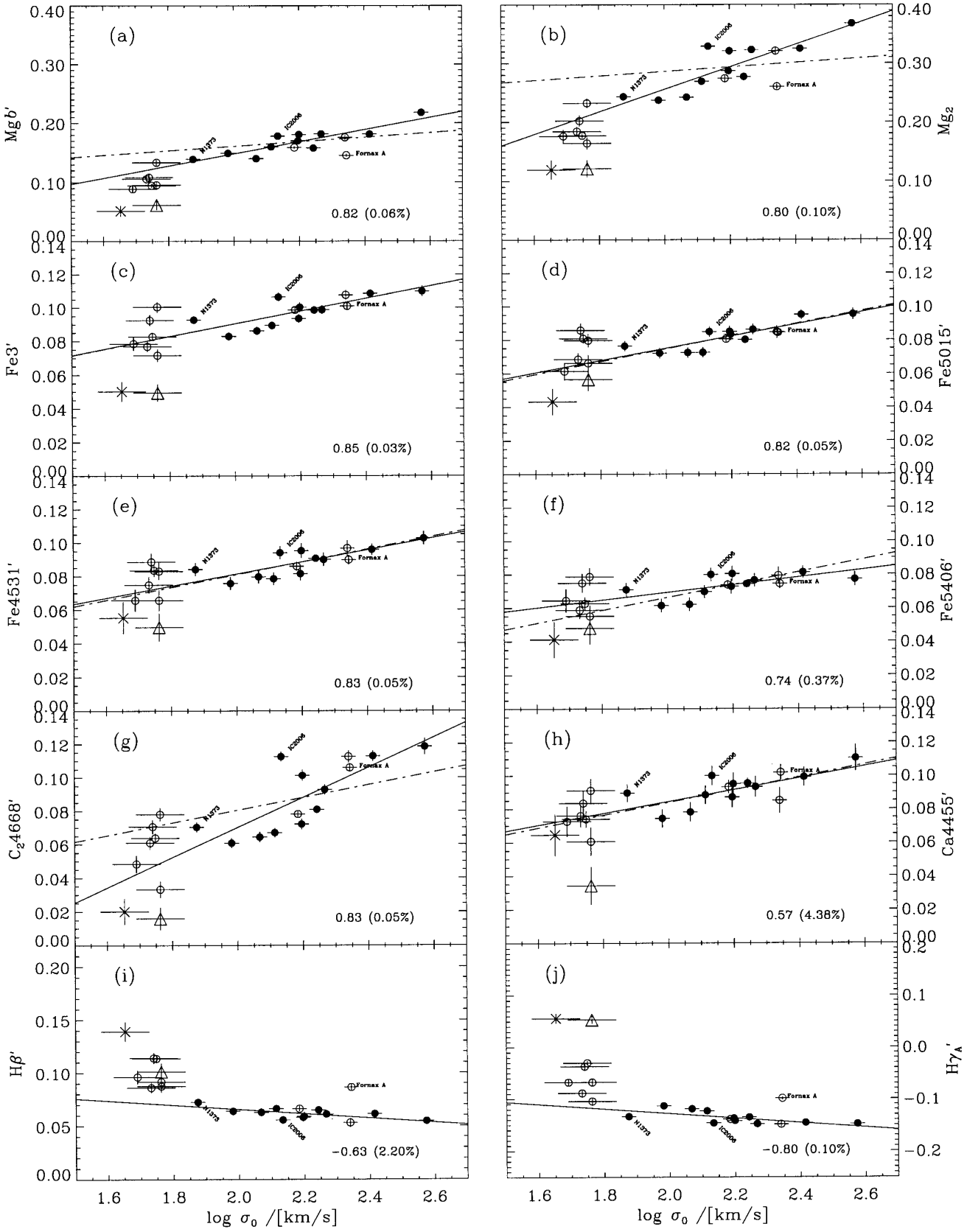

Figure 10. Selected metal absorption indices and Balmer line indices plotted against $\log \sigma_0$. All indices are measured in magnitudes following the conversion from equation (2). Note that all metal indices show a positive correlation and the Fe indices show very similar slopes. The dot-dashed line indicates a slope of 0.035 centred at $\log \sigma_0 = 2.2$. Note that the Mg indices exhibit a much steeper slope. The Spearman rank-order correlation coefficient for each data set is shown with the significance level in brackets in the lower right corner of each panel. All Es and the large S0s NGC 1380 and NGC 1381 were included in the fits.

Table 5. Scaling relations.

index	scatter [mag]
$Mg_2 = (0.191 \pm 0.023) \log \sigma_0 - (0.127 \pm 0.054)$	0.017
$Mg_1 = (0.136 \pm 0.015) \log \sigma_0 - (0.158 \pm 0.035)$	0.014
$Mg\,b' = (0.102 \pm 0.020) \log \sigma_0 - (0.056 \pm 0.044)$	0.011
$C_2 4668 = (0.090 \pm 0.018) \log \sigma_0 - (0.110 \pm 0.042)$	0.012
$Fe3' = (0.038 \pm 0.011) \log \sigma_0 + (0.014 \pm 0.025)$	0.005
$Fe4383' = (0.043 \pm 0.019) \log \sigma_0 + (0.037 \pm 0.045)$	0.007
$Fe4531' = (0.036 \pm 0.010) \log \sigma_0 + (0.009 \pm 0.023)$	0.007
$Fe5015' = (0.036 \pm 0.008) \log \sigma_0 + (0.002 \pm 0.019)$	0.005
$Fe5270' = (0.029 \pm 0.009) \log \sigma_0 + (0.024 \pm 0.020)$	0.004
$Fe5335' = (0.043 \pm 0.009) \log \sigma_0 - (0.017 \pm 0.020)$	0.005
$Fe5406' = (0.023 \pm 0.012) \log \sigma_0 + (0.023 \pm 0.026)$	0.005
$Ca4455' = (0.035 \pm 0.017) \log \sigma_0 + (0.014 \pm 0.038)$	0.009
$H\beta' = -(0.020 \pm 0.007) \log \sigma_0 + (0.106 \pm 0.015)$	0.004
$H\gamma_A' = -(0.045 \pm 0.019) \log \sigma_0 - (0.038 \pm 0.044)$	0.010
$H\gamma_F' = -(0.049 \pm 0.017) \log \sigma_0 + (0.018 \pm 0.037)$	0.009

Note – Errors are estimated by a jack-knife error analysis.

Table 6. Scaling relations – comparison of slopes with Jørgensen (1997, 1999).

index	our data	literature	reference
$\log\langle Fe\rangle$	(0.209 ± 0.047)	(0.075 ± 0.025)	(1)
		(0.084 ± 0.042)	(2)
$\log H\beta_G$	(-0.081 ± 0.042)	(-0.231 ± 0.082)	(1)
		(-0.169 ± 0.038)	(2)
$\log C_2 4668$	(0.429 ± 0.096)	(0.63 ± 0.06)	(1)

References: (1) Jørgensen (1997, 11 nearby clusters)
(2) Jørgensen (1999, Coma cluster)

et al. 1990, hereafter OLS(Y|X)). Included in the fit are all galaxies with old stellar populations, i.e., all Es plus the bright S0s NGC 1380 and NGC 1381, in total 13 galaxies. The 1σ scatter around the relation was robustly estimated by deriving a value which includes nine out of 13 galaxies (69 per cent). A correlation coefficient derived from a (non-parametric) Spearman rank-order test is given in the lower right corner of each panel in Fig. 10. The probability that the parameters are not correlated is given in brackets.

For the galaxies with old stellar populations the Mg–σ_0 relation is in excellent agreement with the literature (Jørgensen 1997; Colless et al. 1999). *Remarkably*, the Fe-line-indices also show a clear positive correlation with the central velocity dispersion and little scatter. This is the first time that such strong correlations have been found at a significant level. We note that all the Fe-line and Ca4455–σ_0 relations show a slope consistent with a value of $\sim$0.035. In contrast, the slope of the Mg lines and $C_2$4668 are significantly steeper (see dot-dashed line in Fig. 10 and Table 5).

Although our Mg_2–σ_0 relation agrees well with those in the literature, we find significant differences for other log(*index*)–σ_0 relations compared to the data of Jørgensen (1997, 1999). Table 6 shows a comparsion of the slopes. The log($\langle$Fe$\rangle$)–σ_0 relation seems to be far steeper in the Fornax cluster, whereas the $\log H\beta_G$–σ_0 relation is shallower compared to Coma. The $\log C_2 4668$–σ_0 relation in Fornax is marginally consistent with Jørgensen (1997). It is not clear why the log (*index*)–σ_0 relations for $H\beta_G$ and $\langle$Fe$\rangle$ should be different to the Coma cluster. We will present a possible explanantion at the end of this section, and in Section 8 where we discuss our results.

The centres of the two bright and old S0s NGC 1380 and NGC 1381 follow generally well the relation set by the elliptical

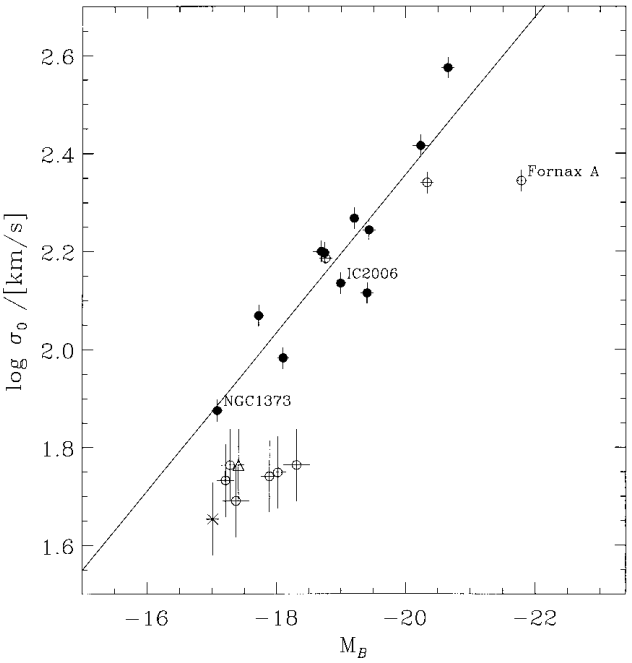

Figure 11. The Faber–Jackson relation for the Fornax sample (assuming $m - M = 31.2$). The magnitudes are taken from the RC3 (de Vaucouleurs et al. 1991). The best linear fit (OLS (Y|X) including all Es and the SOs NGC 1380 and 1381) is shown as a solid line.

galaxies. The lower luminosity S0s have velocity dispersions $\sigma_0 \lesssim 70\,\mathrm{km\,s^{-1}}$ and show a large scatter about the mean relation of the old galaxies. However, it is worth noting that they exhibit generally weak Mg absorption, and some of the faint S0s show as much Fe absorption, as L^* ellipticals. Fornax A, the brightest galaxy in our sample, has a central velocity dispersion of $\sigma_0 \simeq 220\,\mathrm{km\,s^{-1}}$, which is too low compared to ellipticals of this luminosity in the Faber–Jackson relation (see Fig. 11). It also departs significantly from the Mg–σ_0 relations in the sense that it shows too weak Mg absorption. As Fornax A is regarded as the product of a recent merger (Schweizer 1980, 1981; Mackie & Fabbiano 1998), we interpret our results as strong indications of at least one young stellar component in this galaxy.

One would expect the young stars in this galaxy to produce strong Balmer absorption lines (as seen in Fig. 9) and to dilute (or weaken) the metal lines of the underlying older stellar component. However, if the burst mass is not too small, the relative abundances of metal lines should to first order not be affected (see discussion of composite stellar populations in Section 5.3). However, we find that Fornax A deviates only from the Mg–σ_0 relation and not from any of the other metal index–σ_0 relations (Fig. 10). We interpret this as good evidence that the underlying older stellar population of Fornax A is significantly different from ellipticals at this velocity dispersion, i.e., the [Mg/Fe] ratio is lower, close to solar.

Two of the ellipticals stand out from the normal metal index–σ_0 relation: NGC 1373 and IC 2006 (labelled in Fig. 10). These galaxies always show stronger metal-line absorption than what would be expected from the mean relation. This is most prominent in the Fe3′–σ_0 diagram (panel c). We note, however, that the galaxies follow the mean Faber–Jackson relation (Fig. 11). There is little known about the galaxy NGC 1373; perhaps the best explanation why this (elliptical) galaxy is somewhat off the mean relation is to regard it as a transition galaxy between the sequence

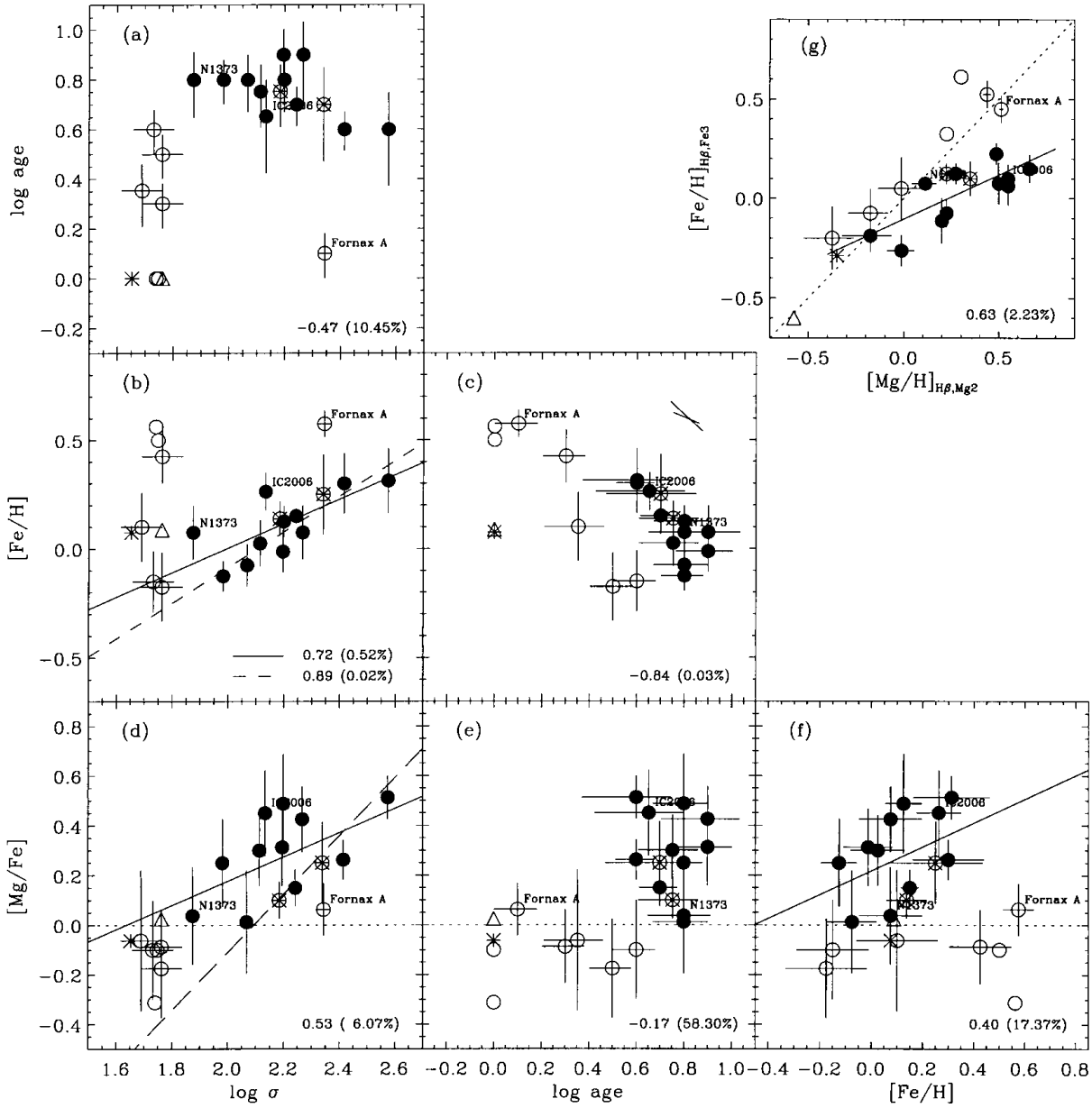

Figure 12. The global relations between log age, metallicity, [Mg/Fe] and log σ_0 are shown. The filled circles represent elliptical galaxies, and the open circles stand for the S0s. The two open circles with a cross indicate NGC 1380 and NGC 1381. ESO 358-G25 and ESO 359-G02 are represented by a triangle and star respectively. For galaxies which lie at the edge or outside the model predictions in the age/metallicity diagnostic diagrams we do not show error bars. A Spearman rank-order correlation coefficient is shown in the lower right corner of each panel (significance in brackets). The Spearman rank-order test includes all galaxies with old stellar populations. The dashed line in panel (b) shows a linear fit excluding NGC 1373 and IC 2006. The long-dashed line in panel (d) shows the relation from Jørgensen (1999) for the Coma cluster. Panel (g) shows the metallicity estimates derived from an Hβ versus Fe3 diagram (y-axis) plotted against the metallicity estimates derived from an Hβ versus Mg_2 diagram (x-axis).

of Es and the faint S0s. However, IC 2006 has been studied in detail by Schweizer, van Gorkum & Seitzer (1989). They found a large counter-rotating ring of neutral hydrogen (H I) associated with faint optical features and suggest that the H I ring may have formed during a merger which created IC 2006. Franx, van Gorkum & de Zeeuw (1994) re-analysed the optical photometry of Schweizer et al. taking into account the inclination of the galaxy, and concluded that it probably has a large disc in the outer parts which is seen almost face-on and therefore difficult to detect. They suggest that it should be classified as E/S0 rather than a bona fide elliptical.

It seems plausible that the (perhaps peculiar) merger history of this galaxy is the reason for its deviation from the index–σ_0 relations. However, from our data it is not clear whether the stellar populations of IC 2006 are too metal-rich, or whether the central velocity dispersion is reduced compared to other elliptical galaxies of this mass. If indeed this type of galaxy is more frequent in other clusters, such as the Coma cluster (see Jørgensen 1999), it would explain why previous authors did not find a clear correlation of Fe lines with σ_0. A detailed analysis of the kinematics and stellar population of this galaxy could be very valuable for our understanding of how the present early-type galaxies were created.

Panels (i) and (j) in Fig. 10 show the index–σ_0 relations for two

Balmer lines. Both indices show negative correlations. Elliptical galaxies and the bulges of NGC 1380 and NGC 1381 show little spread around the mean relation, whereas the younger galaxies, most remarkably NGC 1316, tend to have significantly stronger Balmer absorption at a given σ_0. We emphasize here that the slope in the relation of the galaxies with old stellar populations is mainly caused by a metallicity effect (metal-poorer galaxies have stronger Balmer absorption) and has little to do with age differences. The two 'metal-rich' galaxies IC 2006 and NGC 1373 are deviant from the main $H\gamma_A'$–σ_0 relation in the sense of lower $H\gamma_A$ line strengths. This is caused by the residual metallicity sensitivity of $H\gamma_A$. The side-bands of this index are located on metal lines which lower the pseudo-continuum level and thus weaken the index.

7 GLOBAL RELATIONS

In this section we investigate the relations between our best age, metallicity, [Mg/Fe] estimates and the central velocity dispersions. Fig. 12 presents the results. The ages and metallicities were estimated from a Fe3 versus $H\gamma_A$ age/metallicity diagnostic diagram (Fig. 9) in combination with V96 models. The errors are evaluated following the procedure outlined in Section 5.1, but including only the Poisson error for individual galaxies. Some of the young galaxies are at the edge or outside the range of the model predictions which prevents an accurate error evaluation. For the latter galaxies we do not plot error bars. Notice that the ages and metallicities are derived parameters which carry all the caveats discussed in the previous sections. For example, the independent measurement errors of the line-strength indices translate into correlated errors in the age – metallicity plane due to the residual age/metallicity degeneracy in the Fe3 versus $H\gamma_A$ diagram. We note that the results presented in the following paragraphs would not change significantly if $H\beta$ is used as an age indicator (see Figs C1 and C2 in Appendix C for a comparison of the age and metallicity estimates derived from $H\gamma_A$ and $H\beta$). The Mg overabundance is estimated by evaluating the difference in metallicity estimate between a Mg_2–$H\beta$ and a Fe3–$H\beta$ diagram (see Fig. C3 in Appendix C for an estimation of [Mg/Fe] using $H\gamma_A$).

Our age estimates of ellipticals do not show a significant correlation with $\log \sigma_0$ (panel a). With the exception of Fornax A, all galaxies with $\sigma_0 > 70\,\mathrm{km\,s^{-1}}$ show roughly the same age, whereas the younger galaxies populate the low velocity dispersion range. However, there is a hint that the two dynamically hottest galaxies are younger than their smaller brethren.

For galaxies with old stellar populations there is a clear correlation between the central metallicity and the central velocity dispersion σ_0 (panel b). Consistent with our findings for the Fe3–σ_0 relation the galaxies IC 2006 and NGC 1373 show a stronger metal content than would be expected from the mean relation. The young S0s spread over the whole metallicity range. The best-fitting OLS(Y|X) relation (solid line, jack-knife error analysis) to galaxies with old stellar populations gives

$$[\mathrm{Fe/H}] = (0.56 \pm 0.20)\log\sigma - (1.12 \pm 0.46). \quad (4)$$

A correlation coefficient derived from a Spearman rank-order test (including all ellipticals and the two large S0s) is given in the lower right corner of each panel in Fig. 12. The probability that the parameters are not correlated is given in brackets. Excluding NGC 1373 and IC 2006 from the fit gives the following relation (dashed line in panel b):

$$[\mathrm{Fe/H}] = (0.82 \pm 0.18)\log\sigma - (1.72 \pm 0.40). \quad (5)$$

In the age–metallicity plane (panel c) we find a statistically significant relation in the sense that the more metal-rich (and also more luminous) galaxies are younger. The slope of this relation is similar to what Jørgensen (1999) found for the Coma cluster (see also Worthey, Trager & Faber 1995), yet the Fornax galaxies with velocity dispersion $\sigma_0 > 70\,\mathrm{km\,s^{-1}}$ span a much smaller range in age. We note that the non-treatment of non-solar abundance ratios in combination with correlated errors could be the sole reason for the trend found in Fornax. The direction and magnitude of correlated errors for a galaxy of solar metallicity and 8-Gyr age are shown in panel (c), top right corner. Following on from the age–metallicity relation, Jørgensen (1999) established for the Coma cluster an age–[Mg/H]–σ_0 relation. It would be very interesting to see whether such a correlation exists also in Fornax. However, the small number of galaxies, combined with a rather small spread in age, makes such an analysis very insecure and has therefore not been attempted.

The Mg overabundance shows a weak positive correlation with central velocity dispersion and [Fe/H] in the sense that dynamically hotter and more metal-rich galaxies are more overabundant (panels d and f). In the Fornax cluster significant overabundances are found for galaxies with $\sigma_0 \gtrsim 100\,\mathrm{km\,s^{-1}}$ or $[\mathrm{Fe/H}] \gtrsim 0.0$ (panels f and g). The best-fitting linear relation between [Mg/Fe] and $\log\sigma_0$ is

$$[\mathrm{Mg/Fe}] = (0.49 \pm 0.18)\log\sigma - (0.80 \pm 0.41). \quad (6)$$

This relation is qualitatively in agreement with the results from the Coma cluster (Jørgensen 1999, long-dashed line in Fig. 12d). The scatter about the [Mg/Fe]–σ_0 relation in Fornax is consistent with the errors for [Mg/Fe], but there seems to be a rather large spread in the [Mg/Fe] ratio at a given metallicity (panel f). Although the latter is in good agreement with our findings in the Fe-Mg_2 diagram (Fig. 5), we note that the errors are heavily correlated in the [Mg/Fe]–[Fe/H] diagram. There is no significant correlation of the [Mg/Fe] ratio with log age where the young S0s show solar or slightly less than solar [Mg/Fe] ratios.

8 DISCUSSION

In this study, great care was taken to calibrate the line-strength measurements to a standard system in which we can compare the results with theoretical model predictions (Section 3). The accuracy of this calibration is vital when one wants to derive absolute age and metallicity estimates. Although we were able to demonstrate the high quality of our calibration, some unresolved issues, such as the systematic offset in the Mg_2 versus Mg b diagram, the rather large rms error in the original Lick/IDS stellar library, and perhaps most important of all the largely unknown effects of non-solar abundance ratios, prevent us from deriving accurate absolute age and metallicity estimates. However, for the discussion of *relative* differences in the stellar populations of early-type galaxies our data set and current models are very useful.

In this paper we have made use of two stellar population models provided by W94 and V96. Both models make use of the Lick/IDS fitting functions, but have otherwise somewhat different prescriptions to predict line-strength indices of integrated single-burst stellar populations (SSPs). The predictions of the two models are consistent, and our conclusions would not change if only one of them had been used for the analysis. To our knowledge, this would be also true if we had used any other model which makes use of the Lick/IDS fitting functions.

One of the most important results from this study is the homogeneity of the stellar populations in dynamically hot early-type galaxies in the Fornax cluster. Apart from Fornax A, all early-type galaxies (Es and S0s) with $\sigma_0 > 70\,\mathrm{km\,s^{-1}}$ are of roughly the same age, and their central metallicity scales with $\log\sigma_0$. The homogeneity is reflected in tight relations of observables such as Mg–σ_0 and Fe–σ_0, and a clear correlation of [Fe/H] with the central velocity dispersion. The existence of the latter is reassuring in terms of our current understanding of the colour–magnitude relation (CMR) in clusters being mainly a result of increasing metallicity with increasing luminosity (Kodama & Arimoto 1997; Terlevich et al. 1999).

Previous authors (Fisher et al. 1996; Jørgensen 1997, 1999) pointed out that the lack of a correlation of Fe absorption strength with central velocity dispersion would give evidence for a second parameter or conspiracy of age, metallicity and [Mg/Fe] ratio which keeps the CMR tight. For example, in the Coma cluster Jørgensen (1999) did not find a strong correlation of $\langle$Fe$\rangle$ with central velocity dispersion, and hence her [Fe/H]–σ_0 relation is also not significant. However, both the $\langle$Mg$\rangle$–σ_0 and [Mg/H]–σ_0 relations are clearly seen in Coma. In this context it is important to note that the slope of the Fe–σ_0 relation which one would expect from the change of metallicity in the CMR (Kodama & Arimoto 1997) is quite shallow, and therefore only detectable with high S/N data. In contrast, the Mg–σ_0 relation is steeper, and therefore easier to detect. The reason for this is a combination of a larger dynamical range in the Mg indices compared to the average Fe index and an increasing Mg overabundance with central velocity dispersion giving a steeper slope than would be expected from the change in metallicity only.

An alternative explanation for the lack of a Fe–σ_0 relation in Coma could be based on galaxies such as IC 2006, which do not follow the Fe–σ_0 relation very well. If this type of galaxy is more frequent in the Coma cluster than in Fornax, it would be impossible to find a clear Fe–σ_0 relation. In summary, we find that in the Fornax cluster there is no need for a second parameter such as age, metallicity or [Mg/Fe] to keep the CMR tight. Indeed, we favour an interpretation where small variations of age, metallicity and/or [Mg/Fe] at any given σ_0 are responsible for some real scatter in the scaling relations for the Fornax cluster. However, we emphasize that this may not be true for other (larger?) clusters.

In addition to the population of old, dynamically hot early-type galaxies, we find a sizeable fraction of young, dynamically colder ($\sigma_0 \lesssim 70\,\mathrm{km\,s^{-1}}$) systems within our magnitude-limited survey. Some of the young S0s (NGC 1375, ESO 359-G02 and ESO 358-G25) fit in remarkably well with the predictions of galaxy harassment in clusters (Lake, Katz & Moore 1998; Moore, Lake & Katz 1998). In this scenario, medium-sized disc galaxies (Sc-type) fall into a cluster environment and get 'harassed' by high-speed encounters with cluster galaxies. The end-products are small spheroidal galaxies where some gas of the disc is driven into the centre of the galaxy. This gas is likely to be turned into stars in a central stellar burst. We note that most of these young galaxies are in the periphery of the Fornax cluster, consistent with having been 'accreted' on to the cluster from the field.

Two of the S0s which show young populations in the centre, also have extended discs (NGC 1380A and IC 1963). This seems to be in contradiction with the harassment picture. However, we emphasize that the existing harassment simulations do not include spirals with a substantial bulge component. Here the bulge is likely to stabilize the disc, and the end-products may be able to keep substantial disc components (Ben Moore, private communication). The existence of a population of dynamically colder galaxies with young stellar populations in the nuclear regions is in agreement with a typical (nearby) cluster CMR where one finds a tail of blue galaxies towards the faint end (e.g. Terlevich 1998). Furthermore, Terlevich et al. (1999) demonstrate for the Coma cluster, using line-strength analysis, that these blue galaxies contain young stellar populations rather than being metal-poor.

It seems that in the Fornax cluster significant amounts of young stellar populations are predominantly found in low-luminosity (lenticular) systems. However, for a sample of Coma cluster early-type galaxies Mehlert (1998) found that relatively bright S0s spread over the whole range in age (Es, excluding the cDs, are found to be old). This, of course, raises the question whether morphology is the driving parameter for young stellar populations (only S0s are younger), or whether luminosity is the important parameter (low-luminosity E and S0 galaxies are on average younger). Taking the results from Coma and Fornax together, we would like to argue that in clusters it is only the lenticular galaxies which show signs of recent star formation, and that low-luminosity lenticular systems are more likely to do so. The latter may be just caused by the recent accretion of these low-luminosity systems on to the cluster.

So far we have addressed the age and metallicity distributions in the Fornax cluster with the help of line-strength indices. However, there is more detailed information on the star formation (SF) processes to be gained if one investigates the [Mg/Fe] abundance ratios. When new stars are formed, chemical enrichment is predominantly driven by the ejecta of SN Ia (main producer of Fe-peak elements) and SN II (producing mainly α-elements). However, SN Ia are delayed compared to SN II which explode on short time-scales of $\leq 10^6$–10^7 yr. Taking this into account, there are mainly two mechanisms which determine the Mg/Fe ratio in galaxies: (i) the star formation time-scale and (ii) the fraction of high-mass stars, i.e., the initial mass function (IMF) (see, e.g., Worthey et al. 1992). As re-confirmed in this study, the majority of cluster early-type galaxies show a trend of increasing [Mg/Fe] ratio with central velocity dispersion. Galaxies with young stellar populations and/or low-luminosity galaxies show roughly solar abundance ratios. Given that the most luminous galaxies are also the metal-richest, we emphasize that any realistic star formation models have to be able to produce metal-rich and Mg-overabundant stars at the same time.

In principle, one can reproduce the observed trends of overabundances and metallicity with varying star formation time-scales: *large* galaxies form within *shorter* time-scales than smaller galaxies (Bressan, Chiosi & Tantalo 1996). However, this leads to extremely short star formation time-scales for the most massive galaxies. A plausible way to resolve this dilemma would be a varying IMF where massive galaxies have a top-heavy IMF and low-luminosity galaxies show a more Salpeter-like IMF. For further discussions of the matter see also Tantalo, Chiosi & Bressan (1998) and Peletier (1999).

Recently, Thomas & Kauffmann (1999; see also Thomas 1999) presented preliminary results from their semi-analytic galaxy formation models for the distribution of [Mg/Fe] in galaxies as a function of luminosity. In this scenario luminous ellipticals are the last to form, and hence Thomas & Kauffmann find a trend that the [Mg/Fe] ratio decreases with increasing luminosity, opposite to the observed trend. In general, it seems very difficult with the current stellar population models to reproduce the observed magnesium strength, and therefore [Mg/Fe] values ([Mg/Fe] $\sim$

0.4) of luminous ellipticals (Greggio 1997, but also see Sansom & Proctor 1998).

9 CONCLUSIONS

We have measured the *central* line strength indices in a magnitude limited sample of early-type galaxies brighter than $M_B = -17$ in the Fornax cluster, and have applied the models of W94, WO97 and V96 to estimate their ages, metallicities and abundance ratios. We find the following results.

(i) *Elliptical galaxies* appear to be roughly coeval, forming a sequence in metallicity varying roughly from -0.25 to 0.30 in [Fe/H]. This result is consistent with the conventional view of old, coeval elliptical galaxies where the metallicity scales with the luminosity of the galaxy. This is reflected in scaling relations such as Mg$-\sigma_0$. Remarkably, we could show that all other metal-line-strength indices also clearly correlate with the central velocity dispersion. In fact, all Fe line$-\sigma_0$ relations are consistent with having the same slope.

(ii) *Lenticular galaxies* have luminosity-weighted metallicities spanning the whole range of SSP model predictions. Lower luminosity S0s show *luminosity-weighted ages* less than those of the ellipticals. However, the centres of the bright lenticular galaxies NGC 1380 and NGC 1381 resemble the properties of ellipticals, suggesting that they experienced similar star formation histories. The peculiar S0 galaxy Fornax A (NGC 1316), which is the brightest galaxy in the sample, has strong Balmer lines implying a very young luminosity-weighted age, yet the metallicity is equal to the most metal-rich Es. This is consistent with Fornax A having been involved in a recent gaseous merger. The S0s NGC 1380 and NGC 1381 follow the index$-\sigma_0$ relations of the ellipticals very well. However, the S0s with a young stellar component generally show a large scatter around the scaling relations.

(iii) Our conclusions are based on several age/metallicity diagnostic diagrams which give consistent results. Furthermore, we demonstrate the advantage of using an emission-robust age indicator such as $H\gamma_A$ when analysing the stellar populations of extragalactic objects.

(iv) We have discovered that two of the fainter and very metal-poor lenticular galaxies appear to have undergone major star formation in the last 2 Gyr (in one case very much more recently). We note that, like Fornax A, most of the young galaxies lie on the periphery of the cluster. This is consistent with the harassment picture, where these galaxies are accreted from the field and undergo a morphological transformation with a central star burst.

(v) The elliptical galaxies and the S0 NGC 1380 exhibit overabundances up to 0.4 dex in magnesium compared to Fe. There is a trend that the most massive and metal-rich galaxies are the most overabundant, whereas the fainter Es approach solar ratios. This trend is inconsistent with the currently available semi-analytical predictions for hierarchical galaxy formation. S0s with young stellar populations are consistent with roughly solar abundance ratios, and may even be slightly underabundant. Remarkably also, Fornax A, the brightest galaxy in our sample, shows close to solar abundance ratios which is not what one would expect of an early-type galaxy of its size.

(vi) Furthermore, we note that abundance ratio trends, which are not included in the models, can lead to a change of relative age and metallicity estimates, depending on which index combination is used in the analysis. As long as the non-solar abundance ratios are not properly incorporated into the models, the estimation of absolute ages of integrated stellar populations remains insecure.

ACKNOWLEDGMENTS

I acknowledge the use of Starlink computing facilities at the University of Durham, and also thank the Dr Carl Duisberg Stiftung and the University of Durham for generous financial support during the course of this work. Special thanks are due to Roger Davies, who provided excellent supervision throughout this project. Interesting and very helpful discussions of the following people are acknowledged: Eric Bell, John Blakeslee, Richard Bower, Taddy Kodama, Reynier Peletier, Jim Rose and Alexandre Vazdekis. Thanks also go to Scott Trager and Guy Worthey for providing the Lick/IDS measurements of the higher order Balmer lines. I thank the referee, Inger Jørgensen, for a careful and thorough reading of this paper which helped to improve the final presentation.

REFERENCES

Arimoto N., Yoshii Y., 1987, A&A, 173, 23
Baugh C. M., Cole S., Frenk C., 1996, MNRAS, 283, 1361
Bender R., 1990, A&A, 229, 441
Bender R., Burstein D., Faber S. M., 1993, ApJ, 411, 153
Bender R., Saglia R. P., Gerhard O. E., 1994, MNRAS, 269, 785
Bower R. G., Lucey J. R., Ellis R. S., 1992, MNRAS, 254, 601
Bressan A., Chiosi C., Tantalo R., 1996, A&A, 311, 425
Bruzual G. A., Charlot S., 1993, ApJ, 405, 538
Burstein D., Faber S. M., Gaskell C. M., Krumm N., 1984, ApJ, 287, 586
Burstein D., Davies R. L., Dressler A., Faber S. M., Lynden-Bell D., Terlevich R. L., Wegner G., 1988, in Kron R. G., Renzini A., eds, Towards Understanding Galaxies at Large Redshifts. Kluwer, Dordrecht, p. 17
Caldwell N., 1984, PASP, 96, 287
Cardiel N., Gorgas J., Cenarro J., Gonzalez J. J., 1998, A&AS, 127, 597
Colless M., Burstein D., Davies R. L., McMahan R. K., Saglia R. P., Wegner G., 1999, MNRAS, 303, 813
Davies R. L., Sadler E. M., Peletier R. F., 1993, MNRAS, 262, 650
de Jong R. S., Davies R. L., 1997, MNRAS, 285, 1L
de Vaucouleurs G., de Vaucouleurs A., Corwin H. G., Jr., Buta R. J., Paturel G., Fouqué P., 1991, Third Reference Catalogue of Bright Galaxies. Springer-Verlag, Berlin (RC3)
Edvardsson B., Anderson J., Gustafsson B., Lambert D. L., Nissen P. E., Tomkin J., 1993, A&A, 275, 101
Ferguson H. C., 1989, AJ, 98, 367 (F89)
Fisher D., Franx M., Illingworth G., 1995, ApJ, 448, 119
Fisher D., Franx M., Illingworth G., 1996, ApJ, 459, 110
Franx M., van Gorkom J. H., de Zeeuw T., 1994, ApJ, 436, 642
Gorgas J., Cardiel N., Pedraz S., Gonzalez J. J., 1999, A&AS, 139, 29
González J. J., 1993, PhD thesis, Univ. California
Goudfrooij P., Emsellem E., 1996, A&A, 306, 45L
Goudfrooij P., Hansen L., Jørgensen H. E., Nørgaard-Nielsen H. U., 1994, A&AS, 105, 341
Graham A. W., Colless M. M., Busarello G., Zaggia S., Longo G., 1998, A&AS, 133, 325
Greggio L., 1997, MNRAS, 285, 151
Hau G. K. T., Carter D., Balcells M., 1999, MNRAS, 306, 437
Henry R. B. C., Worthey G., 1999, PASP, 111, 919
Isobe T., Feigelson E. D., Akritas M. G., Babu G. J., 1990, ApJ, 364, 104
Jørgensen I., 1997, MNRAS, 288, 161
Jørgensen I., 1999, MNRAS, 306, 607
Jones L. A., Worthey G., 1995, ApJ, 446, L31
Kauffmann G., 1996, MNRAS, 281, 475
Kodama T., Arimoto N., 1997, A&A, 320, 41

Kuntschner H., 1998, PhD thesis, Univ. Durham
Kuntschner H., Davies R. L., 1998, MNRAS, 295, L29
Lake G., Katz N., Moore B., 1998, ApJ, 495, 152
Longhetti M., Rampazzo R., Bressan A., Chiosi C., 1998, A&AS, 130, 251
Mackie G., Fabbiano G., 1998, AJ, 115, 514
Maraston C., Greggio L., Thomas D., 2000, Ap&SS, in press
McElroy D. B., 1995, ApJS, 100, 105
McWilliam A., 1997, ARA&A, 35, 503
Mehlert D., 1998, PhD thesis, Ludwig-Maximilian-Universiät, München
Moore B., Lake G., Katz N., 1998, ApJ, 495, 139
O'Connell R. W., 1976, ApJ, 206, 370
Oke J. B., 1974, ApJS, 27, 210
Oke J. B., 1990, AJ, 99, 1621
Osterbrock D. E., 1989, Astrophysics of Gaseous Nebula and Active Galactic Nuclei. University Science Books, Mill Valley, CA
Peletier R. F., 1989, PhD thesis, Univ. Groningen
Peletier R. F., 1999, in Beckman J. E., Mahoney T. J., eds, The Evolution of Galaxies on Cosmological Timescales, ASP Conf. Ser. Vol. 187. Astron. Soc. Pac., San Francisco, p. 231
Phillips M. M., Jenkins C. R., Dopita M. A., Sadler E. M., Binette L., 1986, AJ, 91, 1062
Poggianti B. M., Barbaro G., 1997, A&A, 325, 1025
Rose J. A., 1994, AJ, 107, 206
Salaris M., Weiss A., 1998, A&A, 335, 943
Sansom A. E., Proctor R. N., 1998, MNRAS, 297, 953
Schweizer F., 1980, ApJ, 237, 303
Schweizer F., 1981, ApJ, 246, 722
Schweizer F., van Gorkom J. H., Seitzer P., 1989, ApJ, 338, 770
Tantalo R., Chiosi C., Bressan A., 1998, A&A, 333, 419
Terlevich A. I., 1998, PhD thesis, Univ. Durham
Terlevich A. I., Kuntschner H., Bower R. G., Caldwell N., Sharples R. M., 1999, MNRAS, 310, 445
Terlevich R., Davies R. L., Faber S. M., Burstein D., 1981, MNRAS, 196, 381
Thomas D., 1999, MNRAS, 306, 655
Thomas D., Kauffmann G., 1999, in Hubeny I., Heap S., Cornett R., eds, ASP Conf. Ser. Vol. 192, Spectrophotometric Dating of Stars and Galaxies. Astron. Soc. Pac., San Francisco, p. 261
Tonry J. L., Blakeslee J. P., Ajhar E. A., Dressler A., 1997, ApJ, 475, 399
Trager S. C., Worthey G., Faber S. M., Burstein D., González J. J., 1998, ApJS, 116, 1
Tripicco M. J., Bell R. A., 1995, AJ, 110, 3035
van Dokkum P. G., Franx M., 1995, AJ, 110, 2027
Vazdekis A., Casuso E., Peletier R. F., Beckman J. E., 1996, ApJS, 106, 307 (V96)
Visvanathan N., Sandage A., 1977, ApJ, 216, 214
Weiss A., Peletier R. F., Matteucci F., 1995, A&A, 296, 73
Worthey G., 1992, PhD thesis, Univ. California
Worthey G., 1994, ApJS, 95, 107 (W94)
Worthey G., 1998, PASP, 110, 888
Worthey G., Ottaviani D. L., 1997, ApJS, 111, 377 (WO97)
Worthey G., Faber S. M., González J. J., 1992, ApJ, 398, 69
Worthey G., Faber S. M., González J. J., Burstein D., 1994, ApJS, 94, 687
Worthey G., Trager S. C., Faber S. M., 1995, in Buzzoni A., Renzini A., Serrano A., eds, ASP Conf. Ser. Vol. 86, Fresh Views of Elliptical Galaxies. Astron. Soc. Pac., San Francisco, p. 203
Ziegler B. L., Bender R., 1997, MNRAS, 291, 527

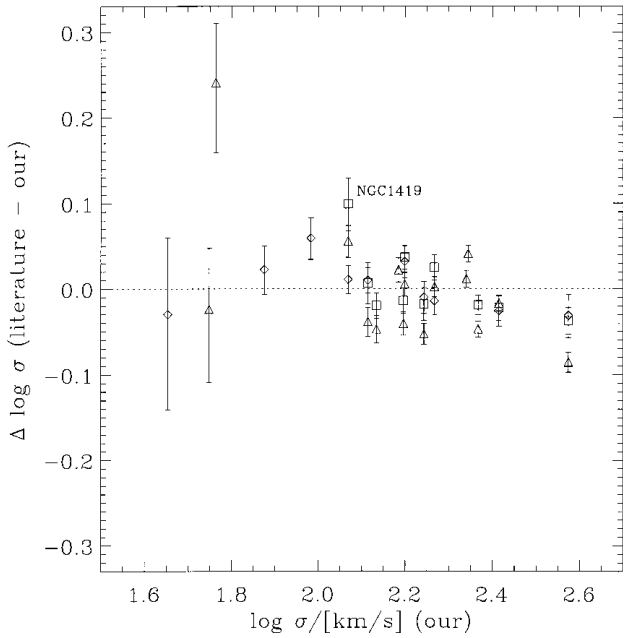

Figure A1. Comparison of our central velocity dispersions with McElroy (1995, triangles), Smith (private communication, squares) and Graham et al. (1998, diamonds). Error bars reflect the literature errors and the rms scatter due to different template stars for the AAT data.

APPENDIX A: KINEMATICS

In Fig. A1 a literature comparison of the central velocity dispersion measurements is presented. The most recent data for Fornax galaxies from Graham et al. (1998) as well as the literature compilation of Smith (1998, private communication) are in good agreement with our data. The comparison with the literature compilation by McElroy (1995) shows a somewhat larger scatter. In order to establish an average error for the velocity dispersion estimates, the mean scatter of the data compared to Smith (private communication) and Graham et al. (1998) is evaluated. For the comparison, all galaxies with $\sigma_0 < 70\,\mathrm{km\,s^{-1}}$ and also NGC 1419 (marked in Fig. A1) from the Smith compilation were excluded. The mean scatter is 0.027 in $\log\sigma_0$. Subtracting in quadrature a mean error of 0.015 for the literature data gives an error of 0.022 [in $\log\sigma_0$] for galaxies with $\sigma_0 \geq 70\,\mathrm{km\,s^{-1}}$. For galaxies with $\sigma_0 < 70\,\mathrm{km\,s^{-1}}$ we adopt the rms scatter of the template stars as estimate of the error ($\Delta\log\sigma_0 = 0.074$).

APPENDIX B: LICK/IDS CALIBRATION

In Fig. B1 a comparison between the original Lick/IDS index measurements of stars and galaxies in common with our data is shown. The individual diagrams show the scatter (Lick/IDS − AAT) around the mean offset versus the average of Lick/IDS and AAT.

Fig. B2 shows the velocity dispersion corrections for each index as derived from broadened stellar and selected galaxy spectra.

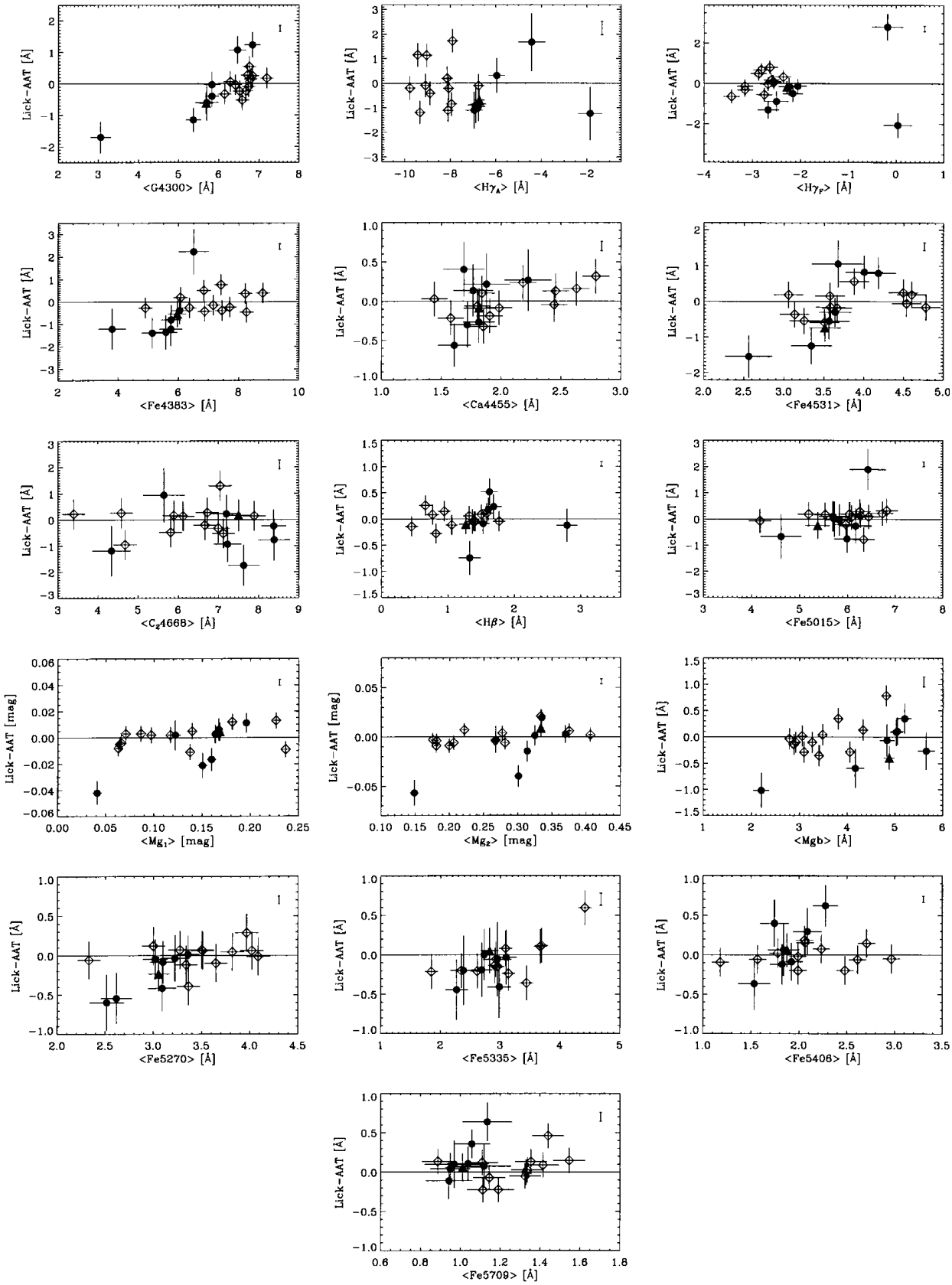

Figure B1. Comparison of 16 indices between Lick/IDS and our measurements *after* the Lick/IDS offset correction (see Table 4) has been applied. Open diamonds, filled circles and the filled triangle represent stars, Fornax galaxies and NGC 3379 respectively. The formal error in the offset is shown as an error bar in the upper right corner of each panel.

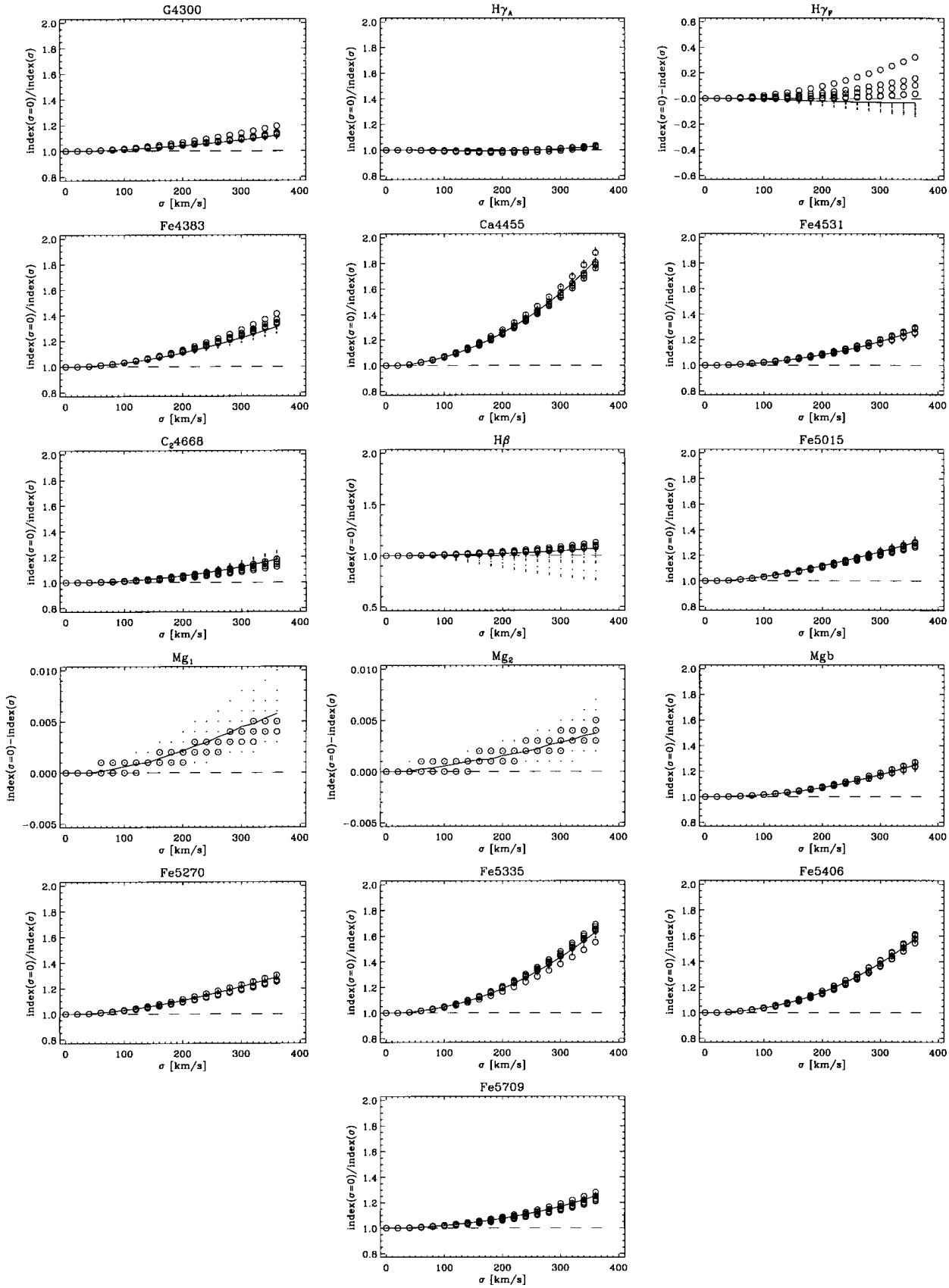

Figure B2. Velocity dispersion corrections. Dots and open circles represent stars and galaxies respectively. The solid line connects the mean of all data points in each σ-bin. Note that for Hβ only stars with equivalent width of H$\beta > 1.1$ Å have been used to determine the mean. See text for details.

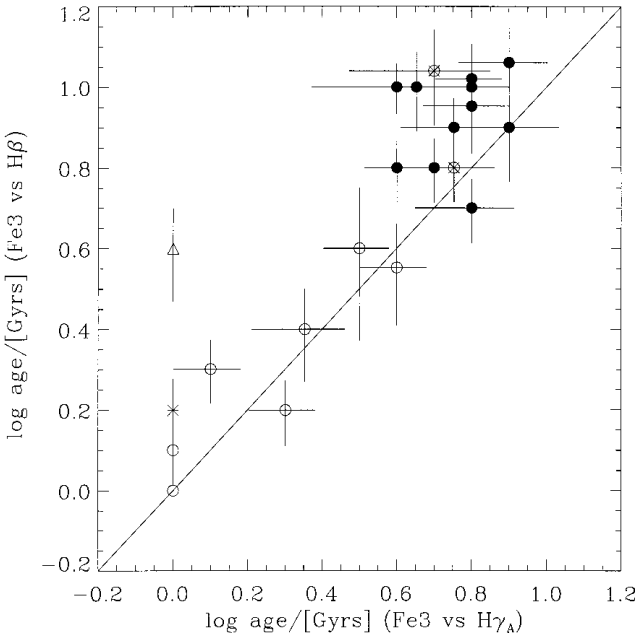

Figure C1. Comparison of the ages derived from a Fe3 versus $H\gamma_A$ diagram and a Fe3 versus $H\beta$ diagram using the models of Vazdekis et al. (1996). For details of the method see Section 5.1.

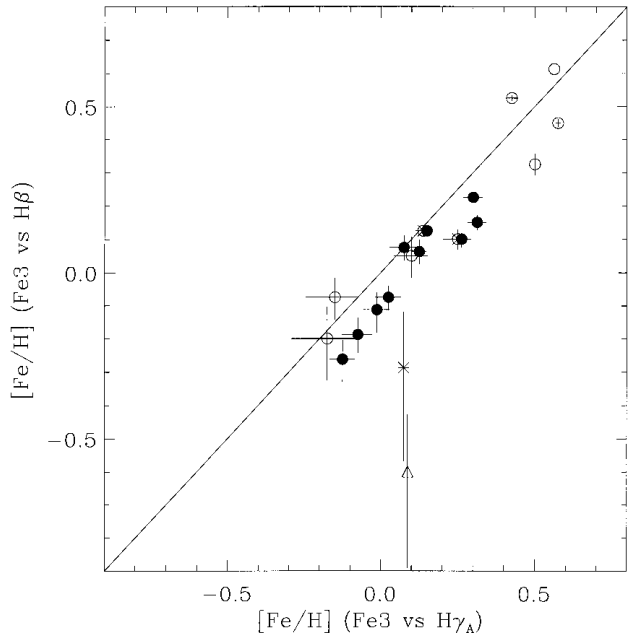

Figure C2. Comparison of the metallicities derived from a Fe3 versus $H\gamma_A$ diagram and a Fe3 versus $H\beta$ diagram using the models of Vazdekis (1996). For details of the method see Section 5.1.

APPENDIX C: COMPARISON OF DERIVED AGES, METALLICITIES AND [MG/FE] RATIOS

Here we present three figures (C1, C2 and C3) comparing our age, metallicity and [Mg/Fe] estimates derived with different index combinations. In general, we find very consistent results when we use, e.g., $H\beta$ instead of $H\gamma_A$ as an age indicator. Most of the differences, such as the [Mg/Fe] ratios of some of the young lenticular galaxies, are caused by the data points lying at the edge of the model predictions or where they have been extrapolated. The extrapolation was necessary, because the models reflect roughly solar abundance ratios and cannot account for, e.g., the strongest Mg_2 absorption found in our sample.

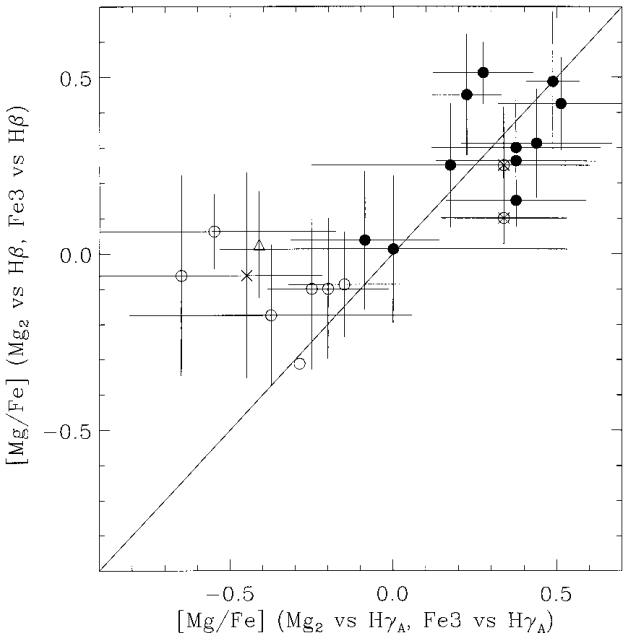

Figure C3. Comparison of the [Mg/Fe] ratios derived from a Fe3 versus $H\gamma_A$, Mg_2 versus $H\gamma_A$ diagram and a Fe3 versus $H\beta$, Mg_2 versus $H\beta$ diagram using the models of Vazdekis et al. (1996). For details of the method see Section 5.1.

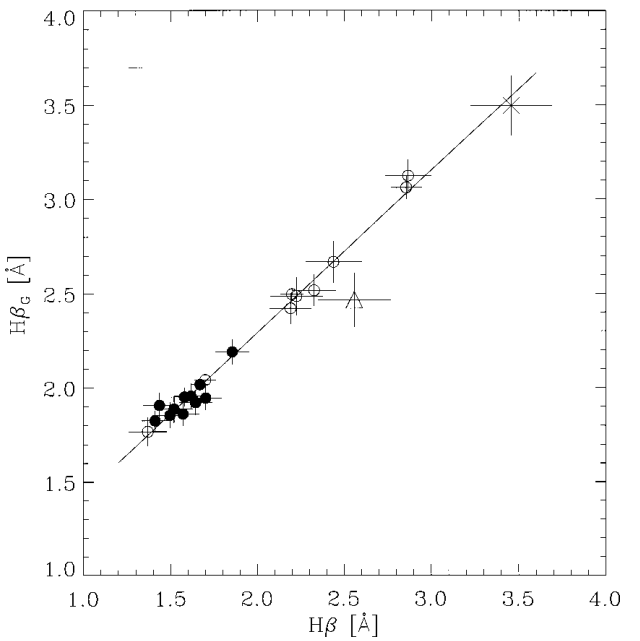

Figure D1. The relation between the Lick/IDS $H\beta$ index and $H\beta_G$ as defined in Jørgensen (1997). The fit includes all galaxies but ESO 358-G25 (open triangle) because of its emission contamination. The error bar in the upper left corner shows the rms error in the offset of the $H\beta$ index to the Lick/IDS system.

APPENDIX D: FINAL CALIBRATED CENTRAL INDICES

D1 Table of central index measurements

The final, fully corrected central (2.3×3.85 arcsec^2) index measurements and associated errors for the Fornax galaxies and NGC 3379 are presented in Table D2. For each galaxy we give our Lick/IDS index measurement in the first row and the 1σ error in the second row. The second column (part 1 of table) lists central velocity dispersions in $\log \sigma$ units. The last column (part 2) lists $H\beta_G$ (not Lick/IDS index); for further details see Section D2.

Table D1. Wavelength definition of $H\beta_G$.

Index	Index bandpass	Pseudocontinua
$H\beta_G$	4851.32–4871.32	4815.00 4845.00 4880.00 4930.00

D2 $H\beta$ versus $H\beta_G$ relation

Fig. D1 shows a plot of $H\beta$ equivalent width versus $H\beta_G$ equivalent width. The bandpasses of the $H\beta_G$ index are defined by Jørgensen (1997), based on an earlier definition of an $H\beta$ emission index by González (1993), in such a way that the influence of the Fe feature right next to the $H\beta$ absorption feature is minimized. For wavelength definitions see Table D1.

The indices $H\beta$ and $H\beta_G$ show an excellent correlation for the Fornax sample. The solid line in Fig. D1 shows the fit to all the data, excluding ESO 358-G25 (open triangle) because of its emission contamination. Using a method which bisects the ordinary least-squares fits made by minimizing the X and the Y

Table D2. Fully corrected Lick/IDS indices for the central (2.3×3.85 arcsec^2) extraction.

Name	$\log \sigma$	G4300 [Å]	Fe4383 [Å]	Ca4455 [Å]	Fe4531 [Å]	C4668 [Å]	$H\beta$ [Å]	Fe5015 [Å]	Mg_1 [mag]
NGC 1316	2.344	5.14	5.95	2.02	3.57	8.02	2.20	5.70	0.119
±	0.022	0.11	0.16	0.09	0.12	0.19	0.07	0.16	0.003
NGC 1336	1.982	5.47	4.85	1.49	3.03	4.70	1.64	4.90	0.097
±	0.022	0.15	0.21	0.11	0.16	0.23	0.09	0.21	0.005
NGC 1339	2.199	5.93	6.15	1.88	3.78	7.69	1.52	5.63	0.168
±	0.022	0.17	0.25	0.14	0.18	0.26	0.11	0.25	0.006
NGC 1351	2.196	6.04	5.56	1.73	3.26	5.54	1.50	5.74	0.137
±	0.022	0.16	0.23	0.13	0.17	0.25	0.10	0.23	0.005
NGC 1373	1.875	5.98	5.83	1.78	3.36	5.41	1.85	5.18	0.101
±	0.022	0.15	0.21	0.11	0.16	0.24	0.10	0.21	0.005
NGC 1374	2.267	6.21	5.80	1.85	3.58	7.07	1.57	5.82	0.164
±	0.022	0.15	0.22	0.13	0.16	0.24	0.09	0.22	0.005
NGC 1375	1.748	3.90	4.40	1.48	3.33	4.93	2.85	5.47	0.062
±	0.074	0.14	0.19	0.10	0.15	0.22	0.09	0.20	0.005
NGC 1379	2.114	5.99	5.37	1.76	3.14	5.16	1.70	4.93	0.121
±	0.022	0.14	0.21	0.11	0.16	0.23	0.09	0.21	0.005
NGC 1380	2.340	5.92	6.26	1.70	3.84	8.50	1.37	5.72	0.161
±	0.022	0.18	0.27	0.16	0.19	0.29	0.11	0.27	0.006
NGC 1380A	1.740	4.16	5.04	1.67	3.53	5.43	2.87	5.79	0.076
±	0.074	0.20	0.28	0.15	0.21	0.32	0.13	0.29	0.007
NGC 1381	2.185	6.09	5.82	1.85	3.42	5.99	1.70	5.45	0.121
±	0.022	0.11	0.15	0.08	0.11	0.16	0.06	0.15	0.003
NGC 1399	2.574	5.90	6.49	2.18	4.06	8.93	1.41	6.41	0.191
±	0.022	0.17	0.29	0.16	0.17	0.39	0.08	0.24	0.004
NGC 1404	2.415	6.03	6.26	1.96	3.81	8.52	1.58	6.39	0.162
±	0.022	0.14	0.20	0.12	0.14	0.24	0.08	0.20	0.004
NGC 1419	2.068	5.75	5.28	1.56	3.18	4.97	1.62	4.92	0.111
±	0.022	0.15	0.22	0.12	0.16	0.24	0.10	0.22	0.005
NGC 1427	2.243	5.95	5.92	1.89	3.61	6.20	1.67	5.43	0.127
±	0.022	0.09	0.12	0.07	0.09	0.14	0.05	0.12	0.003
IC 1963	1.763	5.08	6.03	1.81	3.31	5.98	2.33	5.39	0.093
±	0.074	0.19	0.27	0.14	0.21	0.31	0.13	0.28	0.007
IC 2006	2.134	5.95	6.18	1.98	3.74	8.50	1.44	5.73	0.171
±	0.022	0.15	0.22	0.12	0.16	0.23	0.10	0.22	0.005
E359-G02	1.653	1.64	2.77	1.30	2.23	1.58	3.46	2.97	0.039
±	0.074	0.35	0.50	0.26	0.39	0.61	0.23	0.55	0.013
E358-G06	1.763	5.00	4.05	1.22	2.64	2.60	2.22	4.51	0.057
±	0.074	0.23	0.33	0.17	0.25	0.38	0.15	0.34	0.008
E358-G25	1.763	1.58	2.28	0.70	2.01	1.25	2.56	3.86	0.039
±	0.074	0.30	0.43	0.23	0.34	0.53	0.21	0.47	0.012
E358-G50	1.690	4.85	4.22	1.46	2.64	3.76	2.44	4.18	0.064
±	0.074	0.24	0.35	0.18	0.27	0.41	0.16	0.36	0.009
E358-G59	1.732	5.04	4.84	1.52	3.00	4.71	2.19	4.66	0.067
±	0.074	0.19	0.26	0.14	0.20	0.30	0.12	0.27	0.007
NGC 3379	2.367	6.02	6.30	1.90	3.92	7.48	1.33	5.56	0.166
±	0.022	0.15	0.23	0.13	0.16	0.24	0.09	0.21	0.004

Table D2 – *continued*

Name	Mg_2 [mag]	Mg b [Å]	Fe5270 [Å]	Fe5335 [Å]	Fe5406 [Å]	Fe5709 [Å]	$H\gamma_A$ [Å]	$H\gamma_F$ [Å]	$H\beta_G$ [Å]
NGC 1316	0.260	4.08	3.10	2.90	1.82	1.04	−4.18	−0.64	2.49
±	0.004	0.08	0.08	0.10	0.07	0.05	0.11	0.08	0.04
NGC 1336	0.237	4.17	2.70	2.33	1.51	0.81	−4.82	−1.34	1.92
±	0.006	0.10	0.12	0.13	0.10	0.08	0.17	0.10	0.06
NGC 1339	0.321	4.99	3.04	2.72	1.96	0.93	−6.11	−1.91	1.89
±	0.007	0.12	0.13	0.16	0.11	0.09	0.20	0.12	0.07
NGC 1351	0.287	4.72	3.03	2.51	1.78	0.98	−5.89	−1.85	1.85
±	0.006	0.11	0.12	0.15	0.11	0.09	0.18	0.11	0.07
NGC 1373	0.243	3.90	2.95	2.29	1.74	0.89	−5.74	−1.55	2.19
±	0.006	0.10	0.12	0.13	0.10	0.08	0.17	0.11	0.06
NGC 1374	0.323	5.01	3.13	2.76	1.87	0.98	−6.40	−2.02	1.86
±	0.006	0.10	0.12	0.14	0.10	0.08	0.17	0.11	0.06
NGC 1375	0.177	2.71	2.88	2.49	1.54	1.08	−1.24	1.06	3.06
±	0.006	0.10	0.11	0.13	0.10	0.08	0.14	0.09	0.06
NGC 1379	0.269	4.45	2.80	2.47	1.71	0.92	−5.26	−1.59	1.94
±	0.006	0.10	0.11	0.13	0.10	0.08	0.17	0.10	0.06
NGC 1380	0.321	4.86	3.24	3.18	1.93	1.00	−6.43	−2.16	1.77
±	0.007	0.13	0.14	0.17	0.13	0.09	0.20	0.13	0.08
NGC 1380A	0.202	3.09	3.01	2.84	1.83	1.01	−1.52	0.96	3.12
±	0.009	0.15	0.16	0.19	0.14	0.12	0.21	0.13	0.09
NGC 1381	0.274	4.42	3.15	2.71	1.80	0.97	−5.99	−1.87	2.04
±	0.005	0.07	0.08	0.09	0.07	0.05	0.12	0.08	0.04
NGC 1399	0.368	5.91	3.36	3.11	1.88	0.83	−6.40	−2.04	1.83
±	0.004	0.16	0.11	0.17	0.11	0.07	0.12	0.14	0.05
NGC 1404	0.325	5.00	3.37	3.14	1.98	0.88	−6.29	−1.99	1.95
±	0.004	0.10	0.10	0.13	0.09	0.06	0.13	0.10	0.05
NGC 1419	0.242	3.93	2.72	2.30	1.53	0.82	−5.08	−1.50	1.95
±	0.006	0.10	0.12	0.14	0.10	0.08	0.17	0.11	0.07
NGC 1427	0.277	4.40	3.13	2.64	1.82	0.99	−5.80	−1.68	2.02
±	0.003	0.06	0.06	0.07	0.05	0.04	0.09	0.07	0.03
IC 1963	0.232	3.76	3.06	2.82	1.92	1.04	−4.41	−0.88	2.52
±	0.008	0.14	0.15	0.17	0.13	0.11	0.22	0.14	0.09
IC 2006	0.329	4.92	3.19	3.17	1.95	0.96	−6.32	−2.13	1.91
±	0.006	0.10	0.12	0.14	0.10	0.08	0.18	0.11	0.06
E359-G02	0.119	1.50	1.87	1.38	1.02	0.77	2.19	2.69	3.50
±	0.016	0.28	0.31	0.36	0.27	0.22	0.33	0.20	0.16
E358-G06	0.164	2.74	2.54	1.95	1.36	0.60	−2.81	−0.07	2.48
±	0.010	0.17	0.19	0.22	0.16	0.14	0.25	0.15	0.10
E358-G25	0.121	1.78	1.99	1.57	1.19	0.52	2.09	1.92	2.46
±	0.014	0.24	0.28	0.32	0.24	0.20	0.28	0.17	0.14
E358-G50	0.176	2.55	2.74	2.34	1.58	0.95	−2.82	0.00	2.67
±	0.011	0.18	0.20	0.23	0.17	0.15	0.27	0.16	0.11
E358-G59	0.184	3.02	2.30	2.11	1.45	0.89	−3.72	−0.49	2.42
±	0.008	0.13	0.15	0.17	0.13	0.11	0.21	0.13	0.08
NGC 3379	0.329	5.13	3.21	2.86	1.89	0.99	−6.39	−2.20	1.80
±	0.005	0.11	0.11	0.14	0.10	0.07	0.16	0.11	0.06

residuals we find:

$$H\beta_G = (0.862 \pm 0.027) \times H\beta + (0.568 \pm 0.051). \quad \text{(D1)}$$

The derived relation (errors from a jack-knife analysis) is in very good agreement with the relation found by Jørgensen (1997).

This paper has been typeset from a TEX/LATEX file prepared by the author.